A TRIDENT SCHOLAR
PROJECT REPORT

NO. 263

Optical Variability of the Chesapeake Bay

UNITED STATES NAVAL ACADEMY
ANNAPOLIS, MARYLAND

This document has been approved for public release and sale; its distribution is unlimited.

20000424 154

USNA-1531-2

REPORT DOCUMENTATION PAGE

Form Approved
OMB No. 074-0188

1. AGENCY USE ONLY (Leave blank)	2. REPORT DATE 8 May 1999	3. REPORT TYPE AND DATE COVERED

4. TITLE AND SUBTITLE
Optical variability of the Chesapeake Bay

5. FUNDING NUMBERS

6. AUTHOR(S)
Coleman, James E.

7. PERFORMING ORGANIZATION NAME(S) AND ADDRESS(ES)

U.S. Naval Academy
Annapolis, MD

8. PERFORMING ORGANIZATION REPORT NUMBER

USNA Trident Scholar project report
no. 263 (1999)

9. SPONSORING/MONITORING AGENCY NAME(S) AND ADDRESS(ES)

10. SPONSORING/MONITORING AGENCY REPORT NUMBER

11. SUPPLEMENTARY NOTES
Accepted by the U.S. Trident Scholar Committee

12a. DISTRIBUTION/AVAILABILITY STATEMENT
This document has been approved for public release; its distribution is UNLIMITED.

12b. DISTRIBUTION CODE

13. ABSTRACT: This project investigates the seasonal variation in the in-water optical properties of the Chesapeake Bay estuary. Understanding this variability allows for the proper employment of optical measurement techniques as well as a foundation for accurate interpretation of remotely sensed visible imagery. The absorption and scattering properties of the Bay water column can be expected to change with major physical variations. The most significant source of physical variation in the Bay is associated with the fall destratification or mixing event. As autumn progresses, atmospheric cooling causes a temperature inversion in the water column, thereby weakening the salinity-stratified pycnocline. Combining this inversion with increased winds associated with fall storm systems causes a top to bottom mixing of the water column. An intensive study combining *in situ* hydrographic and optical measurements as well as laboratory characterization of the suspended load is performed across a destratification event in the northern Bay. These data and analysis are combined with theoretical modeling to characterize the physical variation in terms of changes in the absorption, scattering, and hence suspended load properties of the Bay.

14. SUBJECT TERMS
Chesapeake Bay, destratification, ocean optics

15. NUMBER OF PAGES

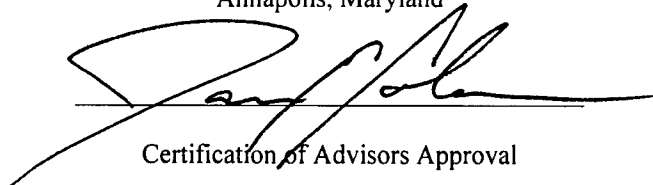**16. PRICE CODE**

17. SECURITY CLASSIFICATION OF REPORT	18. SECURITY CLASSIFICATION OF THIS PAGE	19. SECURITY CLASSIFICATION OF ABSTRACT	20. LIMITATION OF ABSTRACT

Optical Variability of the Chesapeake Bay
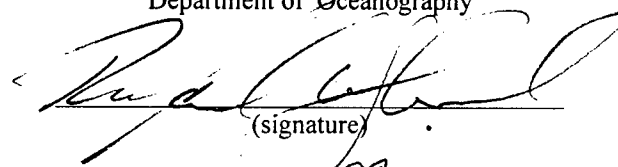
by

Midshipman James E. Coleman, Class of 1999
United States Naval Academy
Annapolis, Maryland

Certification of Advisors Approval
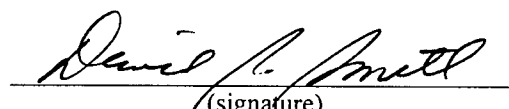
Adjunct Associate Professor Richard W. Spinrad
Department of Oceanography

_____
(signature)

7 MAY 99
(date)

Associate Professor David R. Smith
Department of Oceanography

_____
(signature)

7 May 1999
(date)

Associate Professor Steven N. Montgomery
Department of Physics

_____
(signature)

_5/7/99_
(date)

Acceptance for the Trident Scholar Committee

Professor Joyce E. Shade
Chair, Trident Scholar Committee

_____
(signature)

8 May 1999
(date)

Abstract

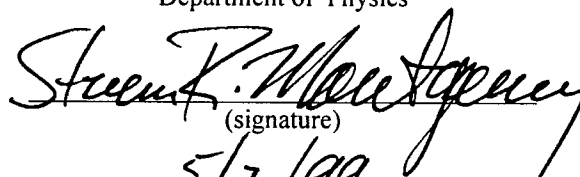This project investigates the seasonal variation in the in-water optical properties of the Chesapeake Bay estuary. Understanding this variability allows for the proper employment of optical measurement techniques as well as a foundation for accurate interpretation of remotely sensed visible imagery.

The absorption and scattering properties of the Bay water column can be expected to change with major physical variations. The most significant source of physical variation in the Bay is associated with the fall destratification or mixing event. As autumn progresses, atmospheric cooling causes a temperature inversion in the water column, thereby weakening the salinity-stratified pycnocline. Combining this inversion with increased winds associated with fall storm systems causes a top to bottom mixing of the water column.

An intensive study combining *in situ* hydrographic and optical measurements as well as laboratory characterization of the suspended load is performed across a destratification event in the northern Bay. These data and analysis are combined with theoretical modeling to characterize the physical variation in terms of changes in the absorption, scattering, and hence suspended load properties of the Bay.

Keywords: Chesapeake Bay, destratification, ocean optics

Acknowledgments

The success of this research is as much a direct result of the wisdom, experience, and generosity of the following people and organizations as it is of my own work. First and foremost I would like to thank Alan Weideman and the NRL Littoral Optics Division Stennis Space Center and the Naval Oceanographic Office for the generous loan of the WETLabs AC-9 instrument used in this study. I also owe considerable thanks to Bill Boicourt, Brian Guarraci, and especially Carole Derry both for sharing and help in correcting the CBOS data set. Emanuel Boss at Oregon State University was kind enough to supply a *Matlab*® code for Mie theory evaluations. I also greatly appreciate the helpful comments and suggestions from Paula Bontempi of the University of Rhode Island and Jennifer Bivens at University of Southern Mississippi. Thank you to Jimmy Asquith, David Smith, and Marge Bem for their patience and ingenuity in surmounting my numerous administrative obstacles.

The time, effort, and ingenuity put forth by Kenny Zepp into ensuring the proper operation of the instrumentation was of paramount importance to the completion of this project. I owe him a lot of credit and gratitude.

Considerable thanks to Reza Malek-Madani for his tremendous help (and patience) both on this project and over the course of the last three years. Finally, I owe a great deal of gratitude to David Smith and Rick Spinrad. Their combined patience and encouragement are the sole cause of the completion of this paper and this project.

Table of Contents

I. Introduction

A. Background

Oceanography, as a natural science, is primarily concerned with the ability to understand the properties of a water body. Achieving this understanding would enable accurate forecasting of system variation, prediction of the impact of these changes on other natural systems, and meaningful assessment of the nature and extent of existing or proposed anthropogenic influences. The consequences of these abilities, of course, are highly influential for both economic and environmental concerns.

Such an understanding of water body dynamics demands both an extensive monitoring capability and an accurate depiction of the interrelationship of water body parameters. Extensive monitoring of the ocean environment is extremely difficult due to the multiple scales of variability involved in oceanic systems. Depicting the interrelationship of water body parameters is equally difficult. The study of optical oceanography promises to contribute significantly to both demands.

Optical oceanography, or ocean optics, as a science, is concerned with accounting for the complete photon budget of a given water body. This requires extensive knowledge of the interaction between light and suspended particles within the water column. These particles include silts, sands, clays, and other input from the land (termed terrigenous) sediments, the diverse suite of suspended plankton (termed biologic), as well as decomposing organic matter (termed detrital). When light impinges upon a suspended particle, the light properties are altered to varying degrees by that particle. The extent of this alteration is dependent upon the ability of that

particle to absorb and scatter light. This ability varies dramatically from terrigenous to biologic and detrital particles, and for particular particles within each of those groups. Thus, as a result of this inherent variability, accurate measurement of the resulting light field can provide extensive information on the physical properties of the particles causing the variation. This defines the significant monitoring capability of optical oceanography, especially when considered along with the ease by which optical measurements can be made both *in situ* and remotely.

The biological structure of most ecosystems, aquatic or otherwise, is grounded in photosynthesis (with a few, almost otherworldly, exceptions). In the marine environment, photosynthesis is highly dependent upon the amount of available light. The small autotrophic organisms, which dominate aquatic photosynthesis, are both highly dependent upon and significantly alter the radiant light distribution. These organisms also have a tremendous effect upon the health, composition, and stability of higher trophic levels and may even alter the physical and chemical properties of their resident water column (Tyler and Seliger, 1989). Thus, comprehension of the photon budget elucidates sources of variation in and helps depict the interrelationship of water body parameters (Kirk, 1994).

A great deal of research has been performed since the 1960's to characterize the sources of variation in the absorption and attenuation (the sum of absorption and scattering effects) of light in the open water environment. These studies have been extremely successful and led to the ability to measure accurately and rapidly global open ocean primary productivity utilizing satellite color imagery (Gordon and Morel, 1983). In these environments the optical properties of the water column are almost

completely correlated to biological activity. Very little quantitative work has been done, however, in aquatic systems with a significant terrigenous input. The Chesapeake Bay, a partially mixed estuary, is just such an aquatic system (Pritchard, 1989). Furthermore, the seasonal variability of optical properties has also been well characterized in the open ocean environment (Gordon, *et al.* 1983). This variability, however, is very limited in scope. The variability in an estuarine system like the Chesapeake is an order of magnitude more intense and diverse. For example, in productive oceanic waters the beam attenuation coefficient, a measure of optical transmission, can vary by as much as 0.5 per meter over 50 meters of the water column (Hamilton, *et al.*, 1990). In the Chesapeake, however, the beam attenuation can change by up to 6 per meter over only 5 meters of depth (Coleman, *et al.*, 1998). This research represents, to the author's knowledge, one of the first truly quantitative insights into the optical dynamics of such an environment.

B. Scientific Question

The greatest degree of optical variability in the Chesapeake should occur across the autumnal mixing, or destratification, of the Bay. In late summer the Bay is a stratified, two-layer system composed of a fresh, riverine surface layer and a salty, oceanic bottom layer. As autumn progresses, the atmosphere cools the fresh surface layer. The bottom, oceanic layer, however, remains warm, creating a temperature inversion within the column. This inversion helps to destabilize the column. Combining this destabilization effect with the increased wind activity associated with autumn storms causes the column to mix throughout, or destratify

(Goodrich, *et al.*, 1987). This vertical mixing not only changes the temperature and salinity of the water column, but also resuspends nutrients, replenishes oxygen, and affects particle-settling rates. All of these changes will impact the composition of the suspended load, and hence should affect the optical properties of the Bay.

Changes in the composition of the suspended load include changes in the index of refraction of the particles comprising the load, changes in concentration, and changes in particle size. All of these changes affect the optical characteristics of the Bay. For example, autumnal mixing results in nutrient resuspension, which in turn causes a significant increase (termed a bloom) in photosynthetic organisms (Smith, *et al.*, 1992). All other variables being constant, this increase in photosynthetic organisms is an increase in concentration of suspended particles. This will increase the attenuation of light within the water column. The photosynthetic properties of the organisms will also increase the proportion of absorption effects over scattering effects contributing to the total attenuation of light (Kirk, 1994). Furthermore, the unique optical properties of the particular size range of particles pertaining to the dominant species of plankton in bloom will have a characteristic effect on the overall optical signal.

The optical coefficients addressed in this study describe how radiant energy is altered throughout a given water column. The radiative transfer equation, utilizing these variables as descriptors of the medium, can integrate these effects to describe the alterations to an incident light beam transiting through the medium. Therefore, with the optical properties of the water column known, radiative transfer can describe the complete radiance distribution resulting from sunlight incident on the water

body's surface. It provides complete information to describe the penetration depths of particular wavelengths of sunlight used for photosynthesis and other photochemical processes, information that is crucial to a complete understanding of water body dynamics. Furthermore, this information describes the radiance distribution leaving the water column. Airborne sensors and satellites can monitor this radiance distribution. These instruments provide a broad monitoring capability unmatched by traditional *in situ* methods. Comprehension of the forward problem given by the radiative transfer equation is essential to solving the inverse problem, or translating a remotely sensed image into the optical properties of the water.

Thus, understanding the nature and extent of optical variability allows for the employment of several powerful monitoring tools. As optical properties are highly dependent on many of the parameters of the water column, monitoring of these properties will elucidate relationships between these multiple parameters. Therefore, understanding optical variability advances the understanding of the estuarine system.

II. Methodology

To obtain an accurate depiction of the optical variability of the Bay, four basic aspects of the variation are explored in this study: the physical variation, the changes in the suspended load, the in-water optical properties (inherent optical properties), and the impact of these properties on the light exiting the water column (apparent optical properties). Understanding all four aspects is critical, as physical variation, namely mixing and stratification processes, drives changes in the suspended load, which in turn drives the variation in the inherent optical properties and affects the apparent optical properties.

A. Physical Variation

Understanding the physical variation of the Bay is essential to interpret properly the source of variation of other parameters. This physical variation includes changes in temperature, salinity, and current structure, and is predominantly associated with atmospheric forcing (Goodrich, *et al.*, 1987). It is changes in these parameters that control the mixing event and subsequent particulate and optical changes. Combined within this physical variation are differences induced by geographic distribution. The effects of the Coriolis force (a result of the earth's rotation) can be expected to produce an east-west component to any variation. Since the Bay is oriented in a north-south direction, the amount of riverine input into the system will also vary along this direction. This may create a north-south aspect of parameter variation. In order to address all aspects of physical variation the study was conducted over the course of three months during the fall of 1998. The primary

focus was an east-west transect of four stations with a secondary emphasis of eight additional stations to maximize geographic coverage. Data collection was temporally spaced such that seasonal, weekly, daily, hourly, and even finer scales of temporal variability could be addressed. In addition to the time-discrete measurements collected on the 19 study days, continuous time-series information was obtained from instrumentation buoys deployed throughout the bay. These buoys were deployed as part of a multi-institutional Chesapeake Bay Observing System (CBOS), managed by the University of Maryland.

Understanding the physical variation in each of the described dimensions will link the forcing mechanisms to the optical variation.

B. Variation in the particle load

Variation of the suspended particulate load must be understood in order to characterize properly the optical variability. With regard to optics, the particulate load has essentially three sources of variability: concentration, index of refraction, and size distribution. A suspended load is comprised of many particles of varying sizes. In most natural waters, to a first approximation, the number of particles per particle-size bin, given by $n(x)$, follows a power law function of x, increasing toward smaller particles:

$$n(x) = Kx^{-m} \tag{1}$$

where x is the particle diameter and K is a multiplicative offset (Bader, 1970). The exponential slope, m, of this distribution is often used to identify the particle-size distribution. Optically, this is significant as different particle sizes attenuate light

with varying efficiencies (van de Hulst, 1957). Beyond variation in the particle-size distribution, the suspended load can also vary in concentration. Such variation has an obvious direct impact upon optical signals. Last of all, the index of refraction of the suspended load can vary. A suspension comprised primarily of photosynthetic organisms will have an index of refraction resulting in significant absorption (similar to a green leaf). On the other extreme, a suspension of terrigenous minerals will have an index of refraction which scatters light to a high degree (e.g., milk of magnesia) but does not absorb (Petzold, 1972). The major classes of suspended particles are biological particles, which are highly absorbing, detrital particles, which absorb strongly in the blue, and terrigenous sediments, which are high scatterers (Jerlov, 1976).

C. Inherent Optical Properties

The optical properties addressed in this study are the beam attenuation coefficient (c), the absorption coefficient (a), and the scattering coefficient (b). These coefficients represent the fraction of a collimated beam of radiant energy that is attenuated, absorbed, or scattered per unit length of the water column (Jerlov, 1976). Generally, the attenuation coefficient is the summation of the absorption and scattering contributions, or simply,

$$c = a + b. \qquad (2)$$

All three variables are affected by the index of refraction of the suspended load, the concentration of particles within the load, and the size distribution of those particles. The specific beam attenuation coefficient (c^*), or the beam attenuation per unit total

suspended volume, can be used to remove the effects of concentration. The phase function, an optical quantity which describes the angular distribution of scattered light, and the backscattering coefficient, which represents the scattering only in the backward hemisphere, are also of considerable importance (Petzold, 1972). From an engineering and instrumentation standpoint, the beam attenuation coefficient is the simplest measurement to take. Hence, understanding physical variation in terms of the beam attenuation coefficient is also of major importance to this study.

The full solution to the equations governing the interaction of an electromagnetic wave incident on a homogeneous sphere was formulated (Mie, 1908). This solution, called Mie theory, can supply the exact phase function, absorption, and scattering coefficients associated with a single particle. This allows for the transition between individual particles and the bulk inherent optical properties of the water column.

Measurements of spectral absorption (a) as well as attenuation (c) coefficients provide a wealth of information about the composition of the suspended particulate load that the beam attenuation coefficient could not provide on its own. Absorption measurements, in this regime, are primarily affected by biological particulates, terrigenous sediments, detrital material, and dissolved humic and fulvic acids. These dissolved acids are termed Colored Dissolved Organic Matter (CDOM), or *gelbstuff* for their yellowish color. The total absorption coefficient is simply the sum of the absorption contributions of its components:

$$a = a_w + a_{bp} + a_{det} + a_{CDOM} \tag{3}$$

where a_w is absorption due to pure water (not relevant for this study), a_{bp} is absorption due to biological particulates, a_{det} is absorption due to detrital particles, and a_{CDOM} absorption due to CDOM. Absorption due to terrigenous sediments has not been studied in detail, but is generally considered part of detrital absorption (Holm-Hansen, 1965). Although these components can be further broken down, that level of detail is not warranted in this study. Knowing the spectral behavior of each component allows the spectral absorption coefficient to be decomposed into its constituent contributions.

D. Apparent Optical Properties

Finally, the impact of optical parameter variation on the ambient radiance distribution leaving the water column (the water-leaving radiance) must be characterized. The radiative transfer equation describes the effect that the various optical coefficients and the phase function will have on a beam of light transiting the medium (Chandrasekhar, 1960). This relationship has powerful consequences for interpretation of remote sensing imagery. Although radiative transfer primarily allows the forward problem to be solved, it can accurately predict whether inversion models should be attempted (from a signal-to-noise standpoint). As most inversion models are highly dependent upon the absorption and backscattering coefficients, the variation of these coefficients becomes considerably important to successful inversion.

By addressing the physical, particulate, inherent and apparent optical variability, a thorough explanation of the nature, extent, and cause of optical variation in the Chesapeake Bay can be reached. This research attempts this explanation by focusing on the variation of these systems around the physical process of destratification.

III. Instrumentation

A diverse suite of instrumentation was utilized for data collection over the course of this study. These instruments fall into three basic categories: *in situ*, laboratory, and remotely sensing instruments. Except where noted, data were collected using the US Naval Academy Oceanography Department Yard Patrol Craft (YP-686). Data were collected at 12 stations in the northern Bay east of the Naval Academy (see Fig 1a-b). These twelve stations were oriented in three east-west transects, with each station in a transect corresponding a bathymetric region of the bay: shallow western boundary, mid-depth, deep channel, and shallow eastern boundary (Fig 1c). Data were collected on 19 days over a three-month span (Table 1).

A. *In situ*

A. 1. Discrete (in-time) hydrography

In situ, basic hydrographic variables were measured continuously over depth using a profiling Seabird® Conductivity, Temperature, and Depth (CTD) instrument. Seabird® CTD models SBE-19 and SBE-25 were used interchangeably during the study. These instruments were calibrated to insure compatibility of data. Conductivity measurements are converted to salinity units by the software associated with the instrument (Seabird Protocol, 1998). The CTD instrument package was lowered through the water column at a rate of approximately 0.5 meters per second. The instrument sampled at 4 Hz, and data were recorded in hexadecimal format.

Data Collected during Fall 1998

Instrument/ Date	CTD	LPC	Spec	ADCP	AC-9	Flor	Stations visited
Aug 25	X	X					9,10,11,12,3
Sep 01	X	X	X				(9,10,11,12)x2
Sep 15	X	X	X				(9,10,11,12)x3 1,2,3,4,5,6,7,8
Sep 16	X	X	X				9,10,11,12
Sep 17	X	X	X	X			9,10,11,12
Sep 18	X	X	X	X			9,10,11,12
Sep 22	X	X	X	X			9,10,11,12
Sep29	X	X	X	X			9,10,11
Sep 30	X	X	X	X		X	(9)x2
Oct 01	X	X	X	X	X	X	(9,10,12,11)x2 1,2,3,4
Oct 06	X	X	X	X	X	X	9,11
Oct 07	X	X	X	X	X	X	10,12
Oct 13	X	X	X	X	X	X	9,10,11,12
Oct 20	X	X	X	X	X	X	9,10,11,12
Oct 27	X	X	X	X	X	X	9,10,11,12
Nov 03	X	X	X	X	X	X	9,10,11
Nov 10	X	X	X	X	X	X	(9,10,11,12)x3 1,2,3,4,5,6,7,8
Nov 12	X	X	X	X	X	X	9,10,11,12
Nov 13	X	X	X	X	X	X	9,10,11,12

Table 1: Data collected over the course of the study.

A. 2. Time-series hydrography

The University of Maryland Center for Environmental Studies (CES) has three moored buoys containing a suite of hydrographic sensors distributed along the Bay as part of the Chesapeake Bay Observation System (CBOS). These buoys are moored in the deep-channel axis of the Bay and span the Bay in a north-south direction (Fig 1a). Each buoy contains atmospheric sensors, and two sets of *in-situ* hydrographic sensors. The upper sensor is 8 ft from the surface and the lower sensor is 8 ft from the Bay floor. The
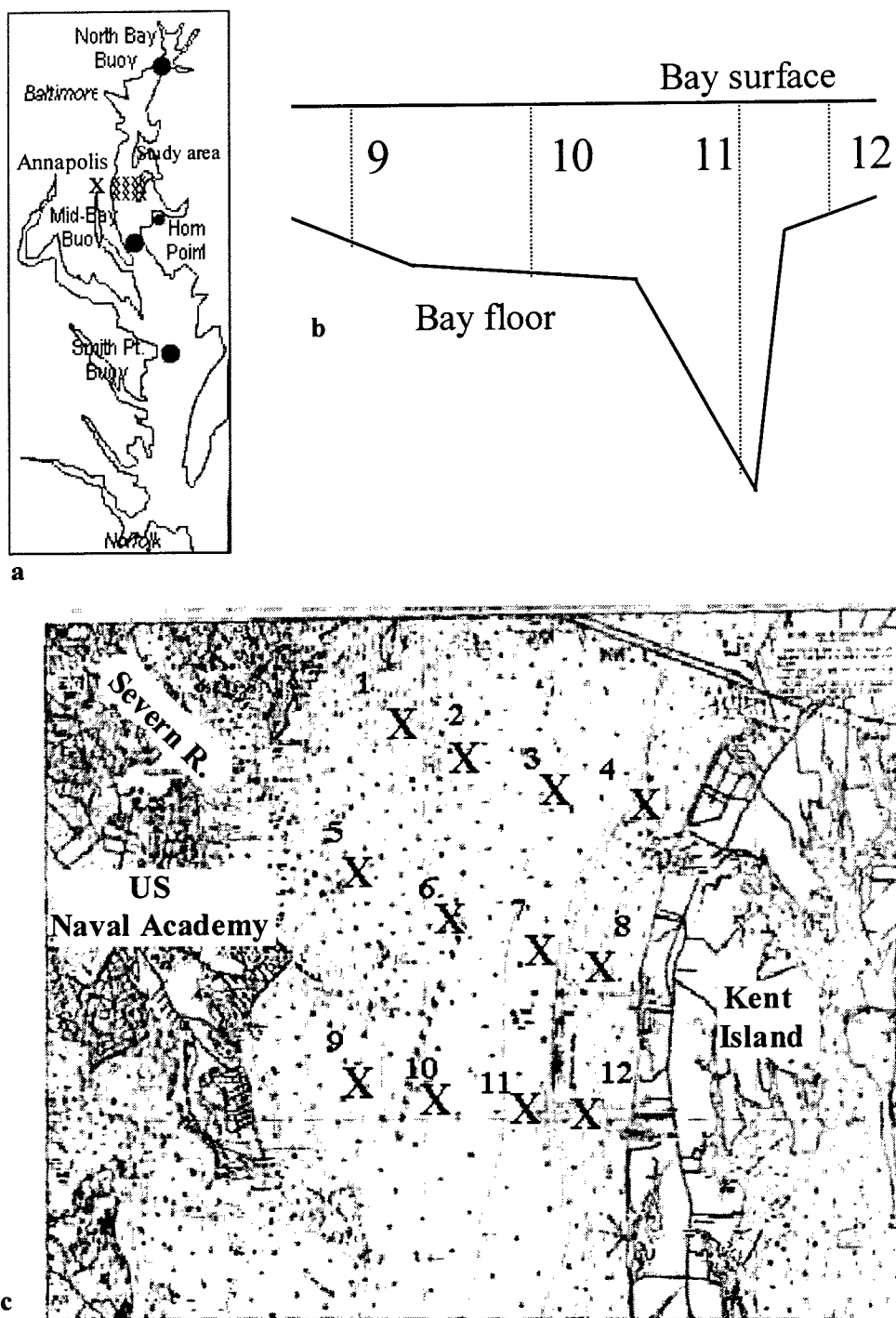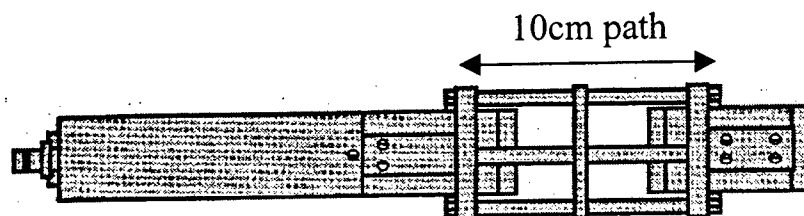
Figure 1: Orientation of the CBOS buoys in relation to the study area, b) bathymetry and stations and c) the study area and station configuration.

10cm path

10 cm Transmissometer Side View

Figure 2: SeaTech transmissometer used to collect beam attenuation measurements at 676nm. The instrument passes a beam through 10 cm of the water column. The upper and lower cans contain electronics.

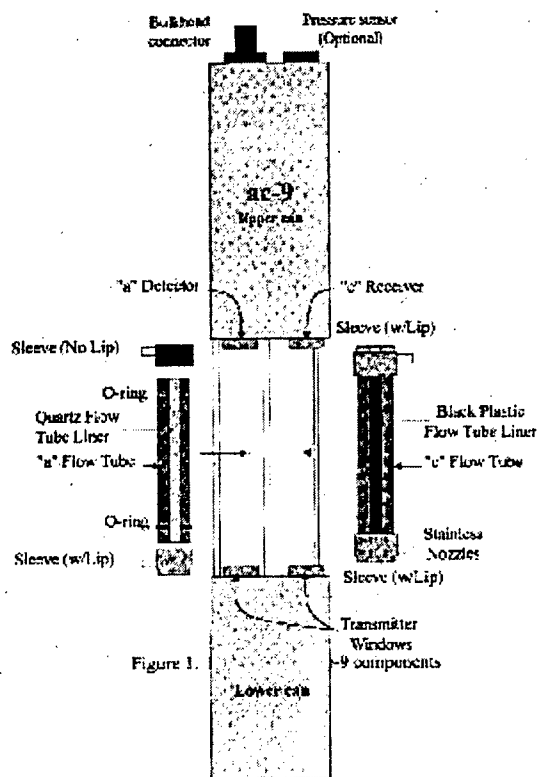Figure 3: WETLabs AC-9 meter. Pumps are used to pass water through the absorption tube (at left) and the attenuation tube (at right). The upper and lower can contain electronics and the internal computer.
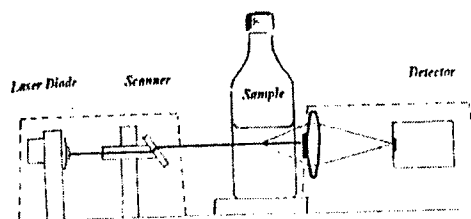

Figure 4: Basic design of the laser particle counter, where a laser is passed through the sample and the near-forward light scatter is collected to be inverted into a particle size distribution

hydrographic suite is composed of Endeco/YSI type SSM conductivity, temperature, and current meters. These instruments recorded data at 10-minute intervals in a block number format. Unfortunately, data from the surface conductivity sensor were unreliable due to the growth of biological matter in the measurement cavity of the instrument (termed biofouling). Wind speed and direction measurements used in this study were made by a B&G wind sensor type 213. The atmospheric data were averaged for 30-minute intervals and were recorded in ASCII format. All time-series data presented in this study were obtained from the mid-Bay buoy located off the mouth of the Choptank River. The remaining buoys were used to qualitatively confirm the application of the processes described by the mid-bay buoy to the full geographic expanse of the Bay (Goodrich *et. al*, 1987).

A. 3. Discrete (in-time) optics

Attached to the CTD unit was a SeaTech® transmissometer (Fig 2). The transmissometer measures the percent transmission of collimated light over a fixed pathlength in the water. The percent transmission is easily converted to a beam attenuation coefficient by the relation:

$$T = e^{-cr} \tag{4}$$

where T is percent transmission and r is the pathlength of the instrument. It uses a stable, well-collimated monochromatic light-emitting diode (LED) with a wavelength band centered at 660nm as a light source. The light is passed through 10 cm of the water column before reaching the photodiode detector. Due to the geometric size of the receiver, it has a one-degree acceptance angle. This imperfection means that the detector

does not measure the true beam attenuation coefficient, but rather includes a very small amount of near-forward-scattered intensity. While significant scatter may occur within the near-forward region (Petzold, 1972), correction for this is difficult and found to be of questionable benefit, especially in highly turbid waters, such as the Chesapeake Bay (Pegau, et al., 1995). Data were acquired in the same manner as with the CTD.

More advanced optical information was collected with the WETLABS AC-9 profiling meter (Fig 3). The particular instrument used in this study (AC9144) is on loan from the Naval Oceanographic Office and Naval Research Laboratories Littoral Optics Division, both in Stennis Space Center, MS. As its name implies, the AC-9 measures absorption (a) and attenuation (c) at nine wavelengths covering the visible spectrum (412nm, 440nm, 488nm, 510nm, 532nm, 555nm, 650nm, 676nm, and 715nm). Unlike the transmissometer, this instrument has a 25-cm pathlength and a 0.7 degree acceptance angle. These differences, however, should cause minimal variation between the two instruments (AC-9 Protocol; WETLabs, 1998). The AC-9 was lowered through the water column by hand, separate from the CTD/transmissometer cast. The AC-9 cast was usually within 5 minutes and 50m of the CTD/transmissometer cast. The instrument internally subtracts the absorption and attenuation effects of pure saltwater. As these values, as well as instrument characteristics, vary with changing salinities and temperatures, the data must be corrected for the environment in which the unit is operated. An additional correction is required to compensate for backscattering effects. As a result of the design of the absorption portion of the meter, the absorption measurements include both true absorption effects (a) and backscattering (b_b). Several methods of correcting backscatter exist and were used in this study (as discussed in

section **IV. A.**). A number of difficulties were encountered over the study period. The pressure transducer on the instrument was engineered for deep-ocean work and, as such, has a resolution of approximately two meters. This was not sufficient for the shallow-water work done in this study. Therefore, depths, as indicated by the meter wheel lowering the unit, were manually recorded in one-meter increments. Additionally, the calibration of the 488nm waveband for beam attenuation drifted considerably over the course of the study, and the data were disregarded. Finally, the cabling used for the instrument was only 25 meters in length. This was sufficient for all but the deep channel stations, where only half the column could be profiled. The instrument was lowered through the water column at approximately 0.25 meters per second. The instrument samples at 4 Hz and data are recorded in ASCII format.

B. Laboratory Instruments

In addition to profiling instruments lowered from YP-686, samples were collected and analyzed using instruments provided by the USNA Hendrix Oceanography Laboratory, which are described in the following sections.

B. 1. Sampling scheme

Discrete water samples were collected by a rosette of Niskin bottles lowered through the water column with or immediately after the CTD/transmissometer. Samples were collected from representative layers of the water column as determined by the real-time readout of the CTD/transmissometer cast. These samples were then refrigerated or frozen to preserve particulate distributions.

B. 2. Particle-size distribution

In the laboratory, samples were analyzed for suspended load information using the Spectrex® Laser Particle Counter (LPC) (Fig 4). This instrument passes a rotating HeNe laser (670.8nm) through the sample and measures near-forward-scattered radiant intensity over an angle from 4 to 19 degrees. It then correlates this scattered intensity to a particle size. Integrating that measurement for a specified time results in a particle-size distribution. There are several sources of error for this particular instrument. As a result of the nature of the detector, the instrument can only count one particle at a time. Therefore, it is only effective at very high dilutions (i.e. low concentrations). In this study, dilutions ranged from 10:1 to 100:1. The exponential nature of the particle-size distribution means that dilution may reduce concentrations of the largest particles below threshold. The LPC also assumes an index of refraction for the suspended particles (the exact value of which is considered proprietary by Spectrex®), which may lead to errors in the particle count. A further assumption is that all particles counted are spherical. While this assumption is obviously invalid, its effects become statistically insignificant as the sampling set increases. As the sampling set increases, the scattered light field of randomly oriented particles approaches the scattered light field of spherical particles of equivalent diameter (van de Hulst, 1957). In effect, each particle has an equivalent spherical diameter, which is measured by the instrument.

B. 3. Particulate absorption

The particle load was further analyzed in the laboratory using a Cary 45 spectrophotometer. Following the Quantitative Filter-pad Technique (QFT) developed

by Mitchell (1990) samples were filtered through a 0.45μm Millipore filter to capture the entire particle load. The filters were then placed in the spectrophotometer for analysis of the particulate absorption spectrum in 2nm increments from 315 to 751nm. However, a number of calibration and correction problems exist for this technique. The current methods for correcting the absorption information for light scatter between the filter-pad and the photomultiplier tube are strictly empirical and somewhat inaccurate. Furthermore, proper QFT requires the use of Glass Fiber filters (GF/F). These filters serve to break up cellular structure and thereby provide better absorption measurements. Along these lines, all current empirical correction studies were conducted for GF/F filters (Roesler, 1998). The spectrophotometric analysis provides a wealth of information for future study, however the complexity of data correction did not warrant its use in this study.

C. Remotely sensed measurements -- Current structure

Current structure information was obtained with an RD® Instruments Acoustic Doppler Current Profiler (ADCP). This instrument relates the Doppler shift of acoustic backscatter to current intensity and direction over discrete depth increments. When on station, the instrument records current profiles in three-second bins for approximately five minutes. The resulting data set contains a time series of current profiles as well as echo intensities. Within the bounds of this project, a strict quantitative evaluation of the current intensities is not necessary, therefore the factory calibration was used and no instrument characterization performed. These data were used qualitatively to define the general dynamic boundaries. A more quantitative evaluation may prove valuable for more advanced studies.

IV. Data Processing

As a result of the broad range of instrumentation used and measurements taken over the fall study period, a significant amount of data processing was conducted. All processing was conducted using the software package *Matlab®*. Most of this processing revolved around correcting AC-9 data and matching the other profiling instruments to the AC-9 format.

A. AC-9 data

As mentioned earlier, depths corresponding to the AC-9 measurements were recorded manually through the use of a meter wheel in one-meter increments. The inherent error in this method is that is does not account for lateral drift of the instrument due to current structure. The lateral drift creates a wire angle, making the depth of the instrument shallower than the meter wheel would indicate. To correct for this, a constant angle was assumed, and a simple cosine relation between the sensor depth as indicated by the meter wheel and the actual bottom depth as given by the CTD/transmissometer pressure transducer was used for all depths. As the AC-9 depth resolution was poorest of all the profiling instruments used in this study, the AC-9 depth measurements were used as the boundaries for data-bin averaging. All measurements between each AC-9 recorded depth were averaged and assigned a depth midway through the bin. While several methods of correcting the AC-9 for backscatter exist, unless otherwise specified all AC-9 data presented in this study were corrected using the Zaneveld correction method (Zaneveld *et al.*, 1992). This assumes that no suspended particulates absorb at the 715nm wavelength, which has been found to be reasonable in all previously studied natural

waters. Therefore, any absorption measurements at this wavelength are attributable in their entirety to backscattering. The correction then assumes that the ratio between backscatter (b_b) and integrated scattering (b) is constant in wavelength (λ):

$$b_b(\lambda) = \frac{a(715)}{c(715)} b(\lambda)$$

(5)

This proportion is subtracted from the absorption measurements of the other eight wavelengths (AC-9 Protocol; WETLabs, 1998).

B. CTD and transmissometer data

CTD and transmissometer data were converted to ASCII format and bin-averaged to match the AC-9 depth bins. In order to correct the AC-9 data for temperature/salinity deviations, bin-averaged CTD data were used in conjunction with factory provided correction coefficients and reference temperature/salinity values.

As discussed previously, CTD/transmissometer profiles are the only complete depth-profile measurement of physical variation made in this study. With these profiles, the degree of stratification can be surmised from the strength of the density gradient (termed pycnocline). The Brunt-Vaïsala frequency (N) is a measure of the strength of the pycnocline, where the higher the frequency the stronger the gradient and, therefore, the more stratified the column. The Brunt-Vaïsala frequency is determined by:

$$N^2 \cong g\left(-\frac{1}{\rho}\frac{\partial \rho}{\partial z}\right)$$

(6)

where ρ is density, z is depth, and g is gravitational acceleration. However, since

CTD/transmissometer measurements are discrete in time, tidal influences cannot be

removed. At times, these influences can be so great that they completely override the

true stratification. These effects are magnified in shallow water and near lateral

boundaries due to increased boundary layer effects. For example, station 9, a shallow

water station near the western boundary of the Bay (Fig 1b-c), exhibits the possible

extent of tidal induced variation. The significant density change shown in Fig 5 is largely

a function of tidal influence. However, away from these boundaries the effect is not as

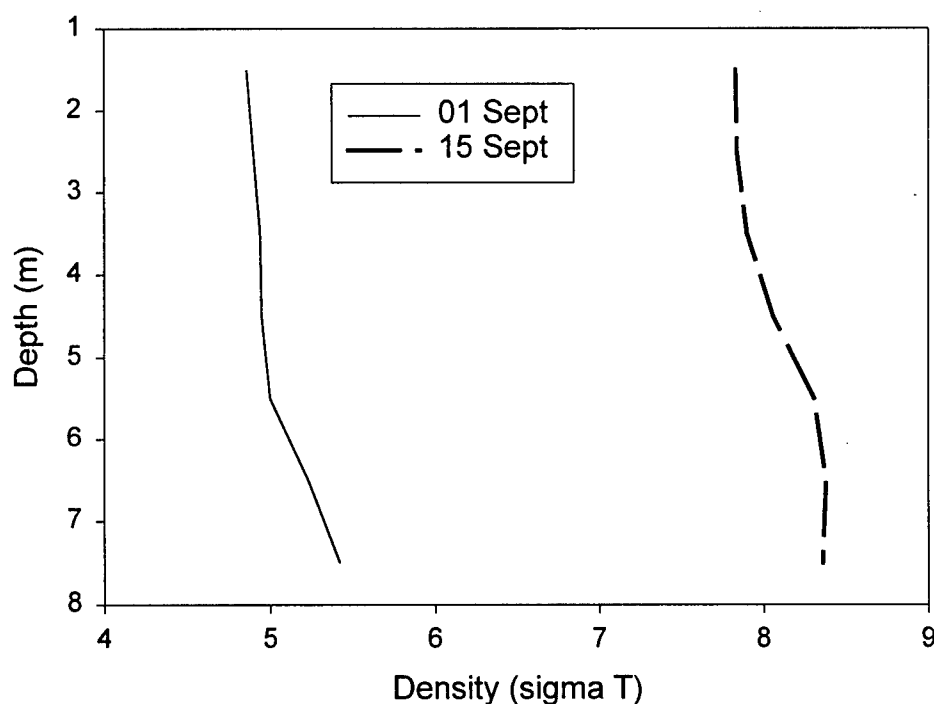significant and useful information can be obtained from the CTD/transmissometer

Figure 5: Change in density at Station 9 from 1-15 Sept. The significant increase in density is attributable to tidal influence.

profiles. As such, station 11, the deep-channel station, is used as a representative station regarding CTD/transmissometer-profile information. All station 11 profiles agree with station 10, the only other weekly station that was not influenced by boundary effects.

C. Time-series data

Time-series information is required to quantify properly destratification. This information was collected by the CBOS mid-bay buoy, located in the deep channel just off the mouth of the Choptank River (Fig 1a-c). This buoy has an instrument suite at 8 ft, which can be considered the surface layer, and at 62ft, or the bottom layer. While this buoy is not located in the study area, the processes involved in destratifying the Bay are on a scale significantly larger than the distance involved here. Furthermore, the mixing event itself occurs simultaneously over large areas in the Bay (Goodrich, *et al.*, 1987). As such, error induced by the geographic separation of the buoy and study area is considered negligible. Due to biofouling in the surface layer salinity meter, vertical salinity differences and density differences could not be computed.

The time-series hydrographic information obtained from the CBOS buoys also required processing. As mentioned earlier, the salinity measurements obtained from the mid-Bay buoy required significant correction due to biofouling. These data were removed from the study. In order to remove astronomical tide variation, a Lanczos low-low pass (LLP) filter with a 34-hour cutoff period was used to reduce the data. As only the along-bay component of the wind and currents are significant for bay dynamics, the raw amplitudes were reduced by the cosine of their direction (due to the north-south

orientation of the Bay). Density was computed using the equation of state for seawater as determined by the International Equation of State (1980).

D. Laser Particle Counter data

Laser Particle Counter data were processed extensively to correct instrumental errors. In order to increase the reliability of the data, all particle counts were performed in triplicate and averaged. Large statistical variation was found for particle counts of less than 15 counts per sample. Therefore, all measurements of less than 15 counts per sample were discarded. Combining this requirement with the exponential nature of natural size distributions and the heavy concentration-dependence of the LPC resulted in a very limited size-range of reliable particle data. On average, reliable data existed for particle sizes ranging from 3 to 15µm. This size range agrees with the range predicted by Bohren and Huffman (1983) for accurate particle sizing using light scattering. As traditionally defined, the smallest suspended particulates are 0.2µm in equivalent spherical diameter (Bader, 1970). These small particles have a significant contribution to the scattering coefficient. At the other extreme, much larger particles, though low in concentration, make a meaningful contribution to the absorption coefficient. Therefore, extrapolation of the particle-size distribution from 0.2µm to 80µm was performed using equation (1) in order to accurately resemble the natural distribution. Particles larger than 80µm were deemed statistically insignificant due to their extremely low concentration.

The model of a single-slope exponential increase in particle counts for smaller particle sizes, called the Junge distribution, is accurate in describing open ocean particle-size distributions. In the Junge distribution, the number of particles of a given size $n(x)$ is

given by equation (1). This exponential Junge distribution has been found to hold true for waters dominated by biological activity. The Chesapeake Bay, however, is considerably more dynamic than the open ocean and, as mentioned earlier, is not entirely dependent upon biological structure for its suspended load characteristics. In such an environment, a two-part, or "kinked" distribution comprised of two exponential slopes may be more appropriate. For this study, both a two-part distribution and a single-slope Junge model were used to compute particle-size distributions. The two-part distribution was computed by segmenting the measured distribution into smaller particle and larger particle distribution, fitting an exponential slope to each segment, and extrapolating that slope to either 0.2 μm or 80 μm. The single-slope distribution, though not as accurate, was used in order to relate findings to other studies (Coleman, *et al.*, 1998). Due to the minimal difference found between the two-part distribution and the single-slope approximation, all particle-size information given in this study is derived from the single-slope approximation. Finally, over the course of the study several shapes of distributions (as measured by the LPC) continually appeared. Therefore, a type number was assigned to each distribution corresponding to the measured shape.

V. Analysis

A. Physical Variation

A. 1. Destratification Mechanisms

Destratification in the Chesapeake Bay requires two basic physical processes to occur: a temperature inversion and a significant wind event. A temperature instability must develop initially in order to weaken the pycnocline for mixing. The first significant wind event following this inversion constitutes the second required physical process. This wind event imparts the energy required for mixing of the water column. Destratification will not occur, regardless of wind event, without the temperature inversion, and hence weaker pycnocline, in place (Goodrich *et al.*, 1987; Vieira, 1986; Irwin *et al.*, 1997).

Full column mixing will temporarily dissipate the vertical salinity and temperature variation. In the absence of a pycnocline, the water column will move as one mass (top and bottom currents in phase), and thereby the vertical current difference will be minimal, whereas during a stratified period the top and bottom currents are often out of phase. Due to the natural tendency of the Bay toward gravitational (i.e. density driven) circulation, a pycnocline, and in particular a salinity gradient (halocline), may reform after the initial mixing, though significantly weakened. The weakened pycnocline will likely persist unless atmospheric forcing returns the top and bottom currents to their stratified (out of phase) condition, strengthening the pycnocline. The phase lag between the top and bottom currents was computed by:

$$p(t) = \frac{\partial w_s}{\partial t} - \frac{\partial w_b}{\partial t} \tag{7}$$

where *p(t)* represents the phase lag equivalent as a function of time *t*, w_s the surface current, and w_b the bottom current. The degree of phase lag can be expected to oscillate in response to new atmospheric forcing and the spring neap tidal cycle. The periodicity of this oscillation is related to the response time of gravitational circulation to a new forcing mechanism. In a column with a weakened pycnocline, the magnitude of gravitational circulation is less (thereby continuing the weakened pycnocline). Gravitational circulation may then be expected to respond more rapidly to a new forcing mechanism. Hence, the periodicity of the phase lag variation may provide information on whether the column is in a mixed, weakened pycnocline state or stratified. This quantity is represented here by the set of times such that:

$$\frac{\partial p(t)}{\partial t} = 0 \qquad (8)$$

and will be termed the periodicity of the phase lag variation.

A. 2. Initial Destratification

Due to variations in atmospheric forcing, the Bay may undergo several cycles of stratification and destratification as autumn progresses (Goodrich *et al.*, 1987; Coleman *et al.*, 1998). The initial destratification, however, is hypothesized to have a greater impact upon the particle load than subsequent events due to the resuspension of nutrients and redistribution of oxygen associated with initial turnover. Therefore, identifying the initial destratification warrants particular attention (though all of the data will be presented simultaneously in Figs 6-9).

A. 2. a. Temperature inversion

The temperature of the surface layer closely mirrored atmospheric temperature patterns at the beginning of the study with the exception of diurnal variability (Fig 6a). A major cold front passed through the study area on 8 September, dropping the surface air temperature as well as the temperature of the upper column. This drop in temperature rapidly leads to an inversion in the temperature structure of the column (Fig 6b). This inversion maintains itself through 16 September, after which the column is mixed as demonstrated by the temperature profile.

A. 2. b. Mixing winds

Two high wind-energy systems passed through the study area during the temperature inversion. The first, and most intense, was associated with the frontal system that initiated the temperature inversion. From 9-11 September gusts exceeded 10 m/s, while the strength of the temperature inversion reached four degrees Celsius with depth (Fig 6b-c). For the duration of this system the winds blew from the north (down the Bay). A weaker period with 4m/s winds followed this storm system. The other wind event that occurred during the temperature inversion spans from 14-15 September. This system was not as intense as the previous storm with gusts averaging 9m/s and, notably, wind direction for this system was from the south (up the Bay).
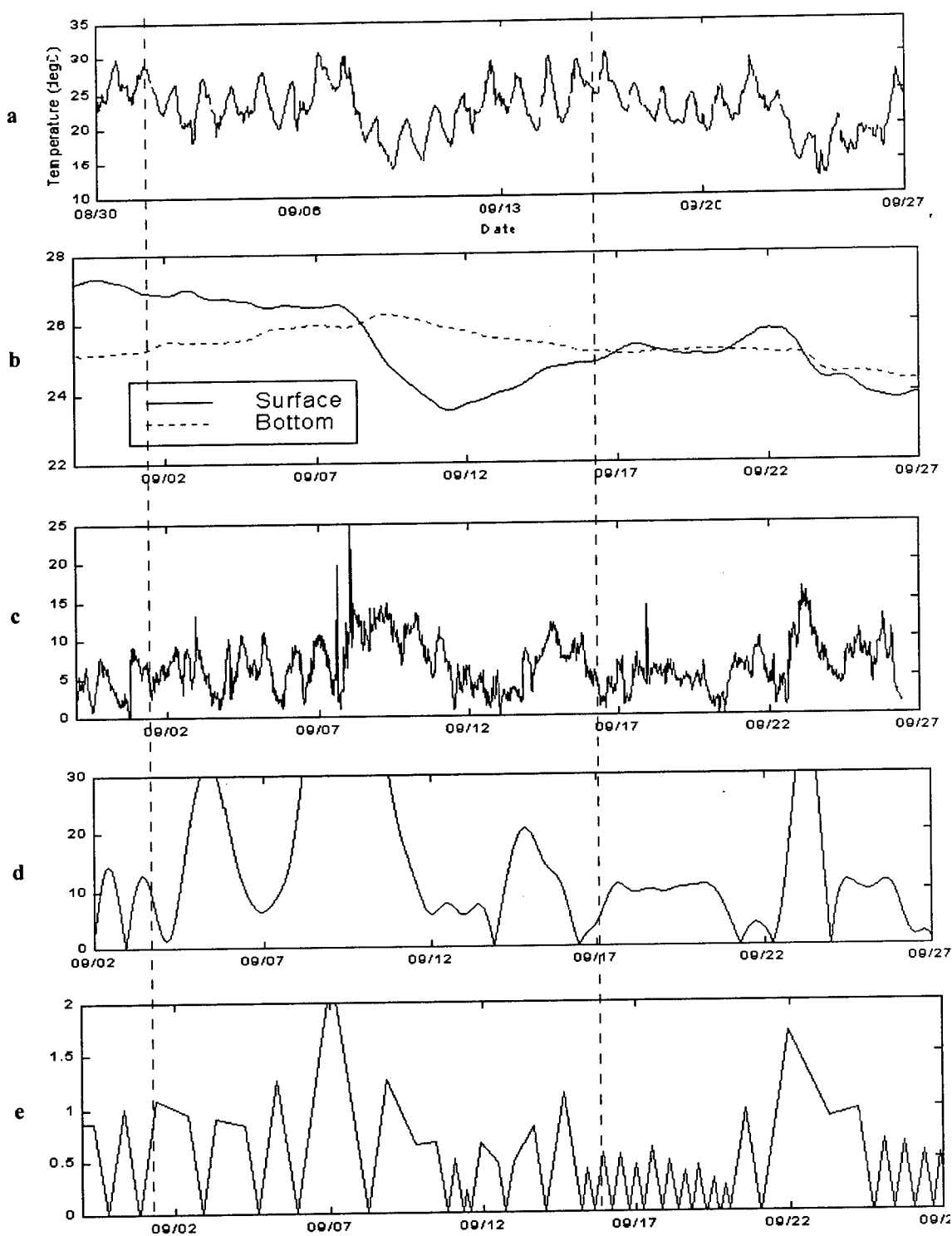
Figure 6: a) Daily atmospheric temperature variation, b) surface and bottom temperatures, c) longitudinal wind magnitude (m/s), d) current shear, and e) phase lag variation. The transects correspond to CTD profiles *aa* and *bb* (see Fig. 9).
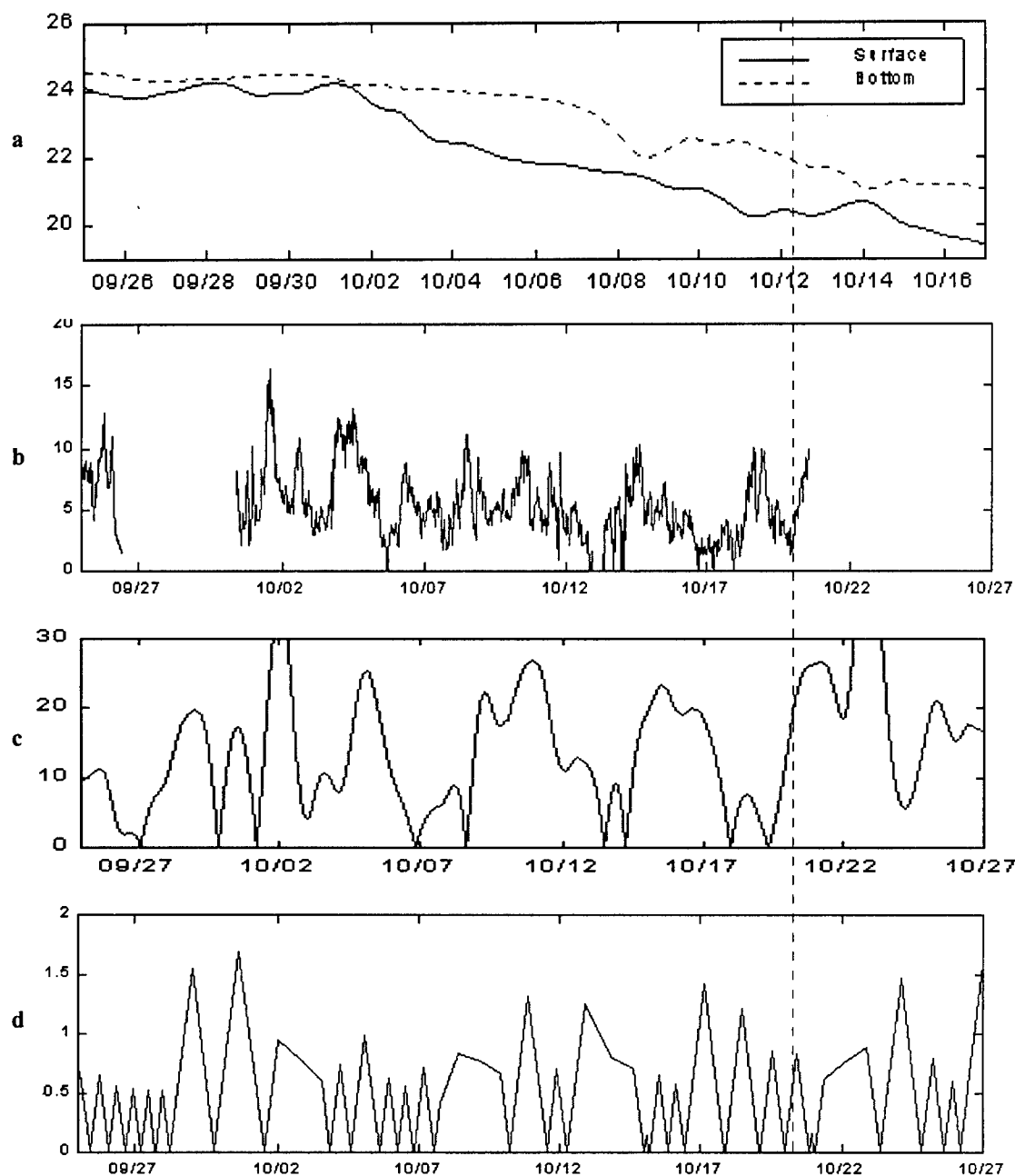
Figure 7: a) surface and bottom temperature, b) longitudinal wind magnitude, c) current shear, and d) phase lag variation for mid-study period. The transect corresponds to CTD profile *cc* (Fig 9). Air temperature data were not available for this time period.
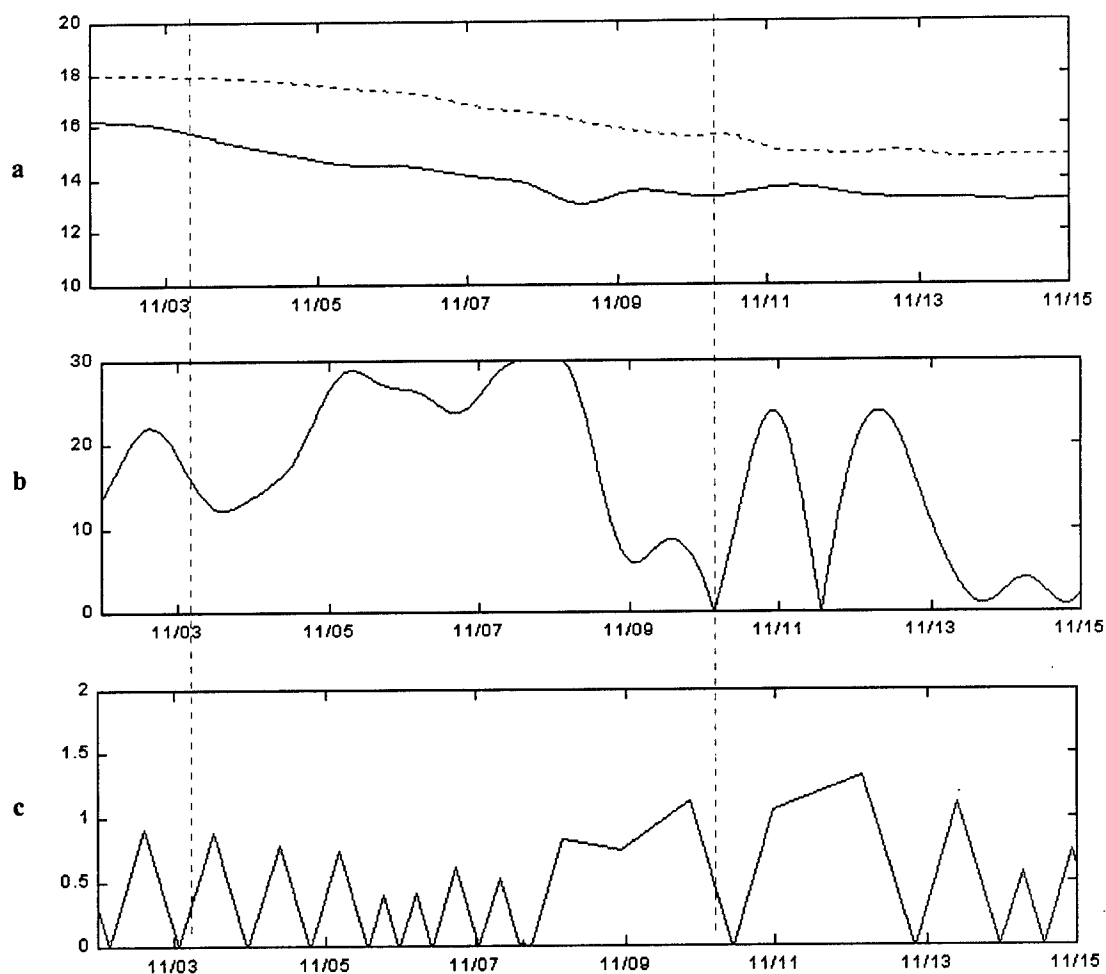
Figure 8: a) Surface and bottom temperatures, b) current shear, and c) phase lag variation for the end of the study period. There were no meteorological data for this period. The 3 Nov transect line corresponds to CTD profile *dd* and *ee* (Fig 9).
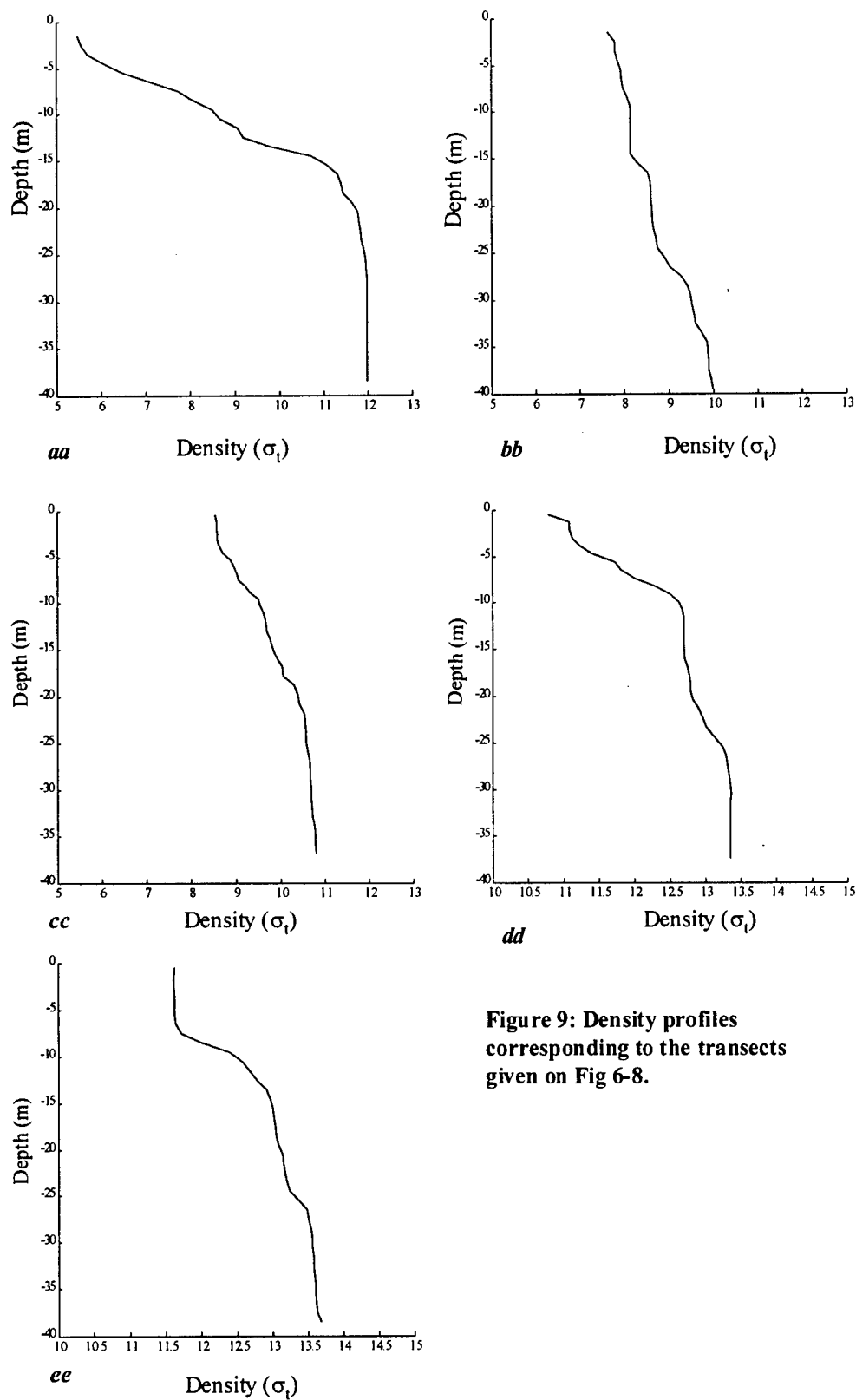
Figure 9: Density profiles corresponding to the transects given on Fig 6-8.

A. 2. c. Hydrographic response

The magnitude of the temperature inversion reached its peak with the passing of the initial storm system on 8 September. The inversion diminished from that point, and is completely dissipated by 16 September (Fig 6b). The 62ft salinity record from the CBOS shows a significant ramping of bottom salinity associated with the 8 September storm system (Fig 10). This reached its peak on 10 September and then freshened until 16 September.
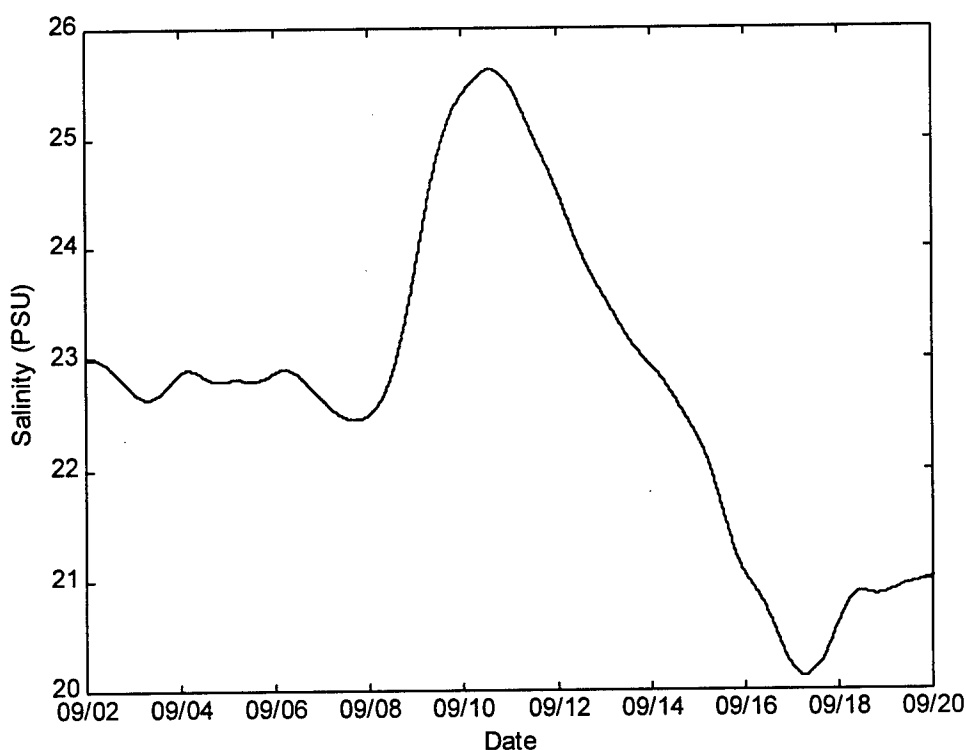
Figure 10: Time-series salinity record at 62 ft for the mid-Bay CBOS buoy. The sudden increase in salinity is associated with the 9 September storm system. The low point in the record occurs on 17 September.

The periodicity of phase lag variation was fairly erratic until 15 September when the frequency increased. At the beginning of the study period the Bay shows strong stratification with a Brunt-Vaïsala frequency of 2.41 mHz as measured from the density

profile in Fig 9aa. The column was stable with respect to both temperature and salinity. While the frequency has dropped slightly (N=1.74 mHz), the column continues to show strong stratification through 15 September. The column is unstable with respect to temperature at this point. On 16 September the Brunt-Vaïsala frequency drops considerably to 0.82 mHz, suggesting stratified conditions no longer persist (Fig 9bb). Temperature and salinity are fairly uniform.

The hydrographic responses suggest destratification occurred between 15-16 September, and not with the more intense storm spanning the 8-11 September. This is likely due to the orientation of the winds during these two systems.

A. 3. Subsequent Mixing/Stratification events

Vertical profiles of temperature remain nearly isothermal through 1 October. The Brunt-Vaïsala frequency of the column has reduced to 0.57 mHz. Additionally, the periodicity of phase variation remains virtually constant (Fig 7d), with the exception of considerable shear following a storm event on about 22 September (Fig 7c). The winds associated with this system exceeded 15 m/s and are from the south (Fig 7b). This shear, similar to that created by the southerly winds on 15-16 September, broke down quickly and re-mixed the slight variation present in the column. The column is then considered as mixed or destratified for this entire period (16 September to 1 October). On 2 October, the top-to-bottom subtidal variation decoupled and became out of phase and the cycles of phase variation behaved somewhat arbitrarily (Fig 7d). This decoupling is associated with a 2 October storm containing gusts from the north exceeding 14 m/s (Fig 7b). These winds are the first northerly winds exceeding 10 m/s since the mixing event of 15-

16 September. These winds partially re-stratified the column. While there are minor mixing events indicated by the current phase and temperature variation, such as on 14 and 19 of October (Fig 7a-c), the column remained essentially stratified from 2-27 October. This is evidenced by the increased periodicity in the phase lag variation and the decoupling of the top and bottom column temperatures (Fig 7a-d). On 27 October the vertical temperatures recouple (Fig 7a). While no data exist for the current variation for the period 27 October - 2 November (Fig 7d-8c), the periodicity of the phase lag variation from 3-7 November resembles the previous mixed phase, suggesting that the column was mixed from 27 October to 7 November. From 7 November to the end of the study the column remained stratified with the Brunt-Vaïsala frequency as high as 0.86 mHz (Fig 9dd).

The CTD is fairly consistent with the time-series information. The CTD data from 13-20 October show only a weak pycnocline during the re-stratified period as depicted by the CBOS data (Fig 9cc). While this is inconsistent, it may be explained by the minor mixing events that occurred in close proximity to those cast dates. The bulk physical variation occurred in the form of a mixing event between the 15-16 September, a well-mixed column through 4 October, and restratified column through 27 October, a mixed column again through 8 November, and a shift to stratification for the remainder of the study.

B. Particle Load Variation

The total suspended volume (TSV) is a measure of the concentration of particulates within the water column. Variation in the TSV over time shows no discernible pattern (Fig 12). Furthermore, the TSV varies widely from depth to depth and station to station for any particular date. The majority of samples were below 100 µL/L TSV, however there continued to be considerable variation from 0-100 µL/L. Averaging over the entire study period, TSV generally decreases west to east (Fig 11), with a considerable difference of 158 µL/L between the average TSV on the western boundary and eastern boundary (stations 9 and 12, respectively).
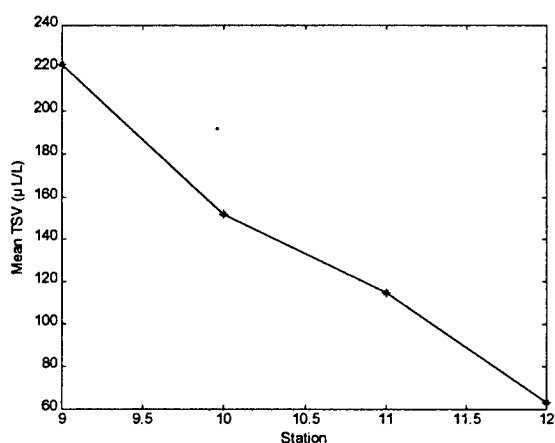
Figure 12: Mean TSV of all data at each station. A distinct decrease in TSV occurs moving from west to east (from station 9 to 12).

Similar to the total suspended volume, the particle-size distribution showed no discernible pattern in time or in depth, with the exception of a reduction in variability mid-course of the study (Fig 13). In the east-west direction, the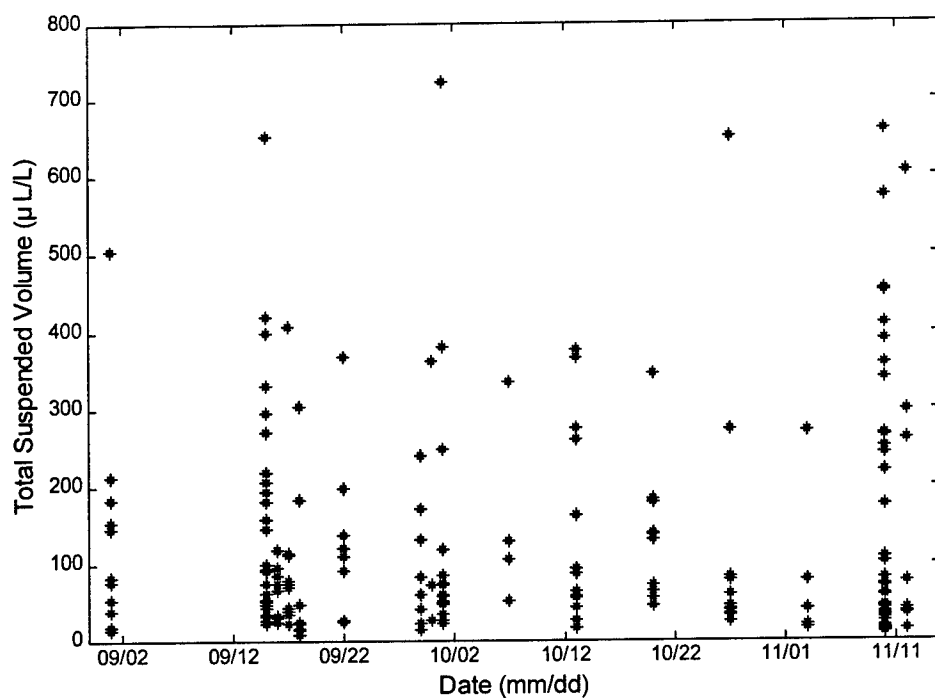 particle distribution changed steadily from a distribution skewed toward larger particles on the western boundary to higher slope, smaller particle distributions on the eastern boundary (Fig 14). Therefore, smaller particles comprise an increasingly significant percentage of the particle size distribution from the western to the eastern boundary of the Bay.

The total suspended volume shows a strong dependence upon the particle-size distribution (Fig 15). Modeling the relationship between TSV and PSD suggests that the

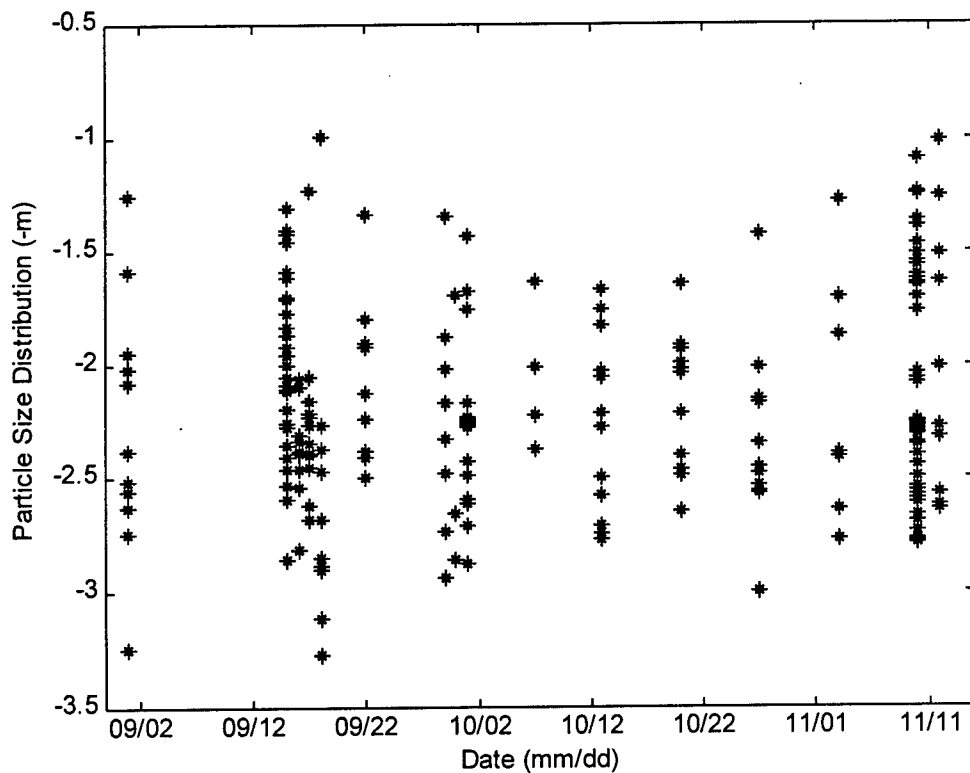**Figure 12: Time history of TSV shows no appreciable trend during the observation period.**

Figure 13: Time history of PSD shows a decrease in variability mid-study as the only appreciable trend.

particle-size distributions in this study are being altered by the addition or subtraction of

large particles. The total suspended volume is given by:

$$TSV = \sum_{i=1}^{N} n(x_i) \cdot \frac{1}{6} \pi \cdot x_i^3 \tag{9}$$

where x is the equivalent spherical diameter and $n(x)$ the number of particles of size x for

a distribution of sizes ranging from x_i to x_N. As stated previously, the particle-size

distribution is given by:

$$n(x) = Kx^{-m} \tag{10}$$

where holding K constant and allowing m to vary generates several particle size

distributions with the same y-intercept. This family of distributions has very similar

concentrations of small particles but widely varying large particle concentrations. The

relationship between TSV and PSD for this type of PSD variation is very similar to the

PSD/TSV relationship observed during the study (Fig 16). If K is allowed to vary with m

such that the large particles are held constant, or:

$$K = \frac{k}{x_N^{-m}} \tag{11}$$

where k is a constant, the PSD/TSV relationship becomes the inverse of the observed

relationship. Similarly, rotating the particle-size distribution around its central point (i.e.

mid-size particles) by using:

$$K = \frac{k}{x_{\left(\frac{N+1}{2}\right)}^{-m}} \tag{12}$$

does not yield a TSV/PSD relationship resembling the observed Chesapeake relation (Fig

16).

Therefore, concentration and particle-size distribution vary somewhat randomly in depth and time in the Chesapeake during the study period. The majority of this variation is due to the addition and removal of larger particles.
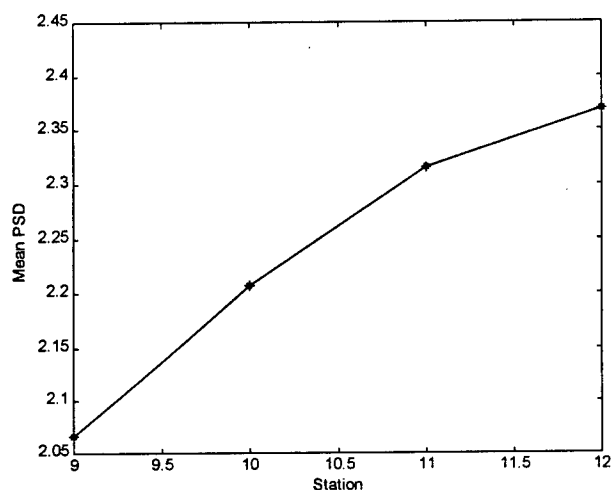

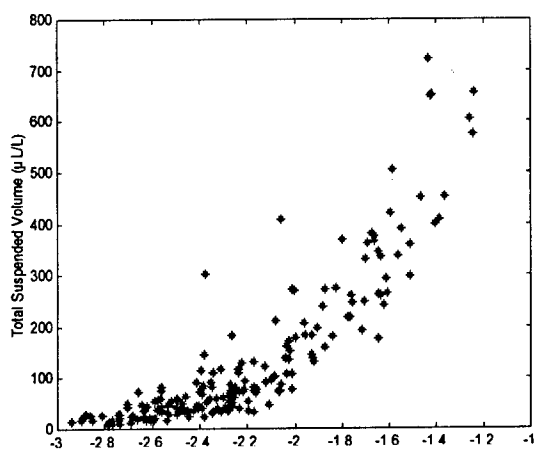**Figure 14: Mean PSD (*m*) of all data at each station.**
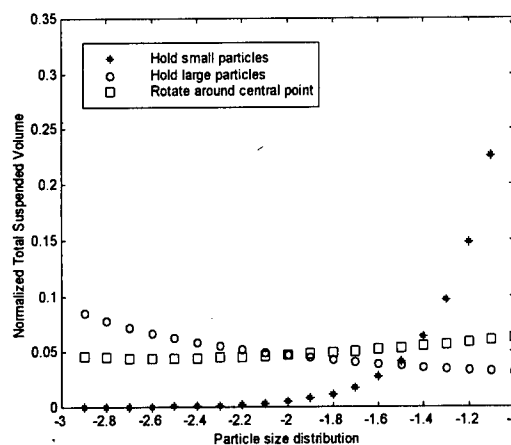

Figure 15: TSV vs. PSD showing a clear dependence.

Figure 16: Modeled relations between TSV and PSD. Clearly the relation created by holding small particles constant and allowing larger particles to vary most resembles Fig 15.

C. Beam Attenuation Variation

As described earlier, for a given particle-size distribution and index of refraction, a linear relationship should exist between beam attenuation coefficient and concentration or total suspended volume (Spinrad, 1986). A change in the particle-size distribution or mean index of refraction of the suspended load will change the slope of this relationship.

The profiles of beam attenuation show no appreciable trend over the study period. A decrease in beam attenuation persists over the first few meters of the water column for the majority of profiles. Beyond this surface layer, profiles vary considerably with depth. Beam attenuation does not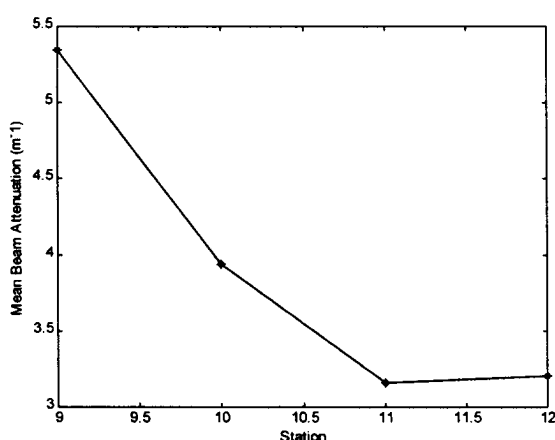 drop below one per meter during the study period. Values typically fall between 2.5 and 4 per meter. The maximum values reach 9-10 per meter. There was also a discernible west-east variation within the data. The western-most stations show significantly higher beam attenuation values than the other stations (Fig 17).

Figure 17: Mean c for all data at each station.

The relationship between TSV and beam attenuation shows discrimination (with significant scatter) for 1-15 September data points (Fig 18a), which represent the stratified period as delineated by the hydrography (phase I). Applying a linear regression to the data yields a slope of 116 μL/L/m^{-1}. While the correlation coefficient, or the r^2 value, is only 0.46, this degree of scatter is expected in the highly variable environment of the Chesapeake Bay (this is described below). Beginning with 16 September, the TSV vs. c slope drops considerably.

From 16 September through 1 October, the data show a slope of 53 μL/L/m^{-1} with an r^2 of 0.51 (Fig 18a-b). From 7-20 October the slope increases slightly to 91 μL/L/m^{-1} and the scatter reduces to an r^2 of 0.65 (Fig 18b-c). After 20 October the slope of correlation drops considerably to 12.3 μL/L/m^{-1} and increases in scatter to an r^2 =0.47 (Fig 18c-d). Following the onset of the final hydrographic phase on 8 November, the slope of correlation rises again to 127 μL/L/m^{-1} with r^2=0.50 (Fig 18d). As a result of the inherently large scatter, these slopes, per se, are not very meaningful but they do indicate meaningful trends in the changing relation over time.
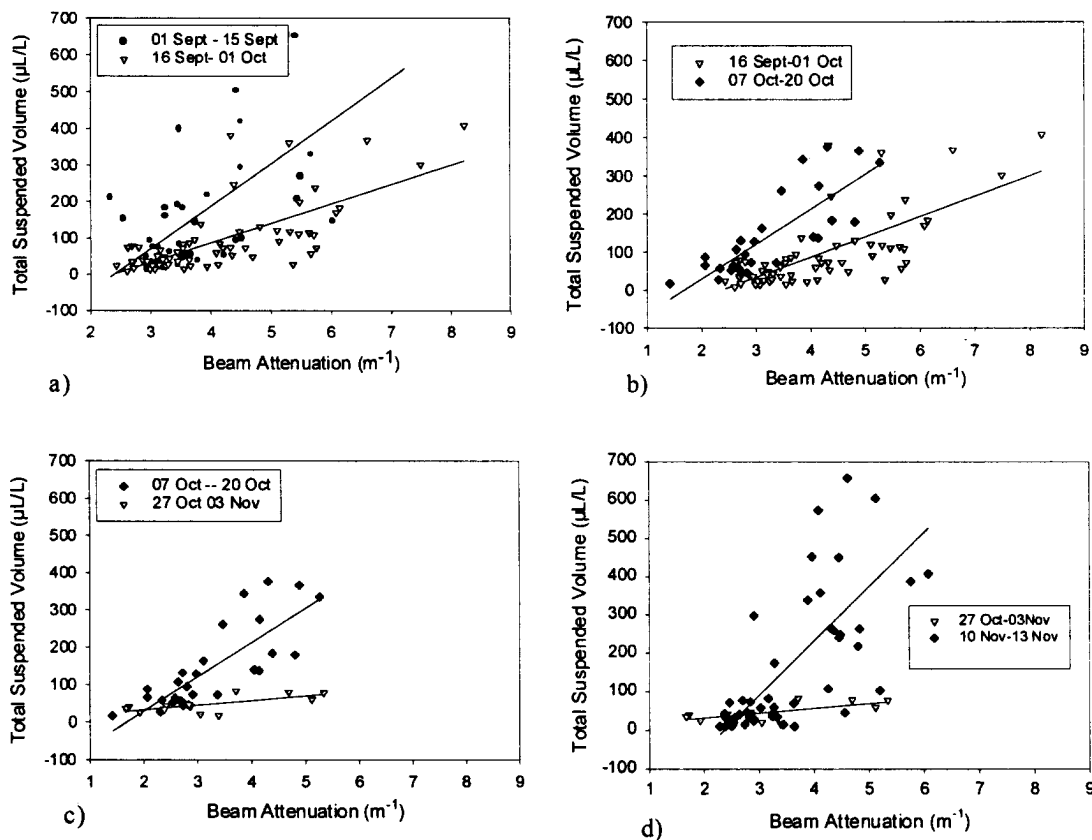

Figure 18: Beam attenuation vs. TSV and regression lines for each of the hydrographic phases: a) shows the transition from phase I to II, b) phase II to III, c) phase III to IV, and d) phase IV to V.

The particle-size distribution shows no appreciable trend in variation either temporally, vertically, or geographically over the course of the study (Fig 19). However, it does exert a strong influence on the specific beam attenuation coefficient (beam attenuation per unit total suspended volume), as shown in Figure 20. As a result of this influence, it is likely the lowered correlation in the relation between beam attenuation and TSV is attributable to the rather stochastic nature of particle-size distributions.
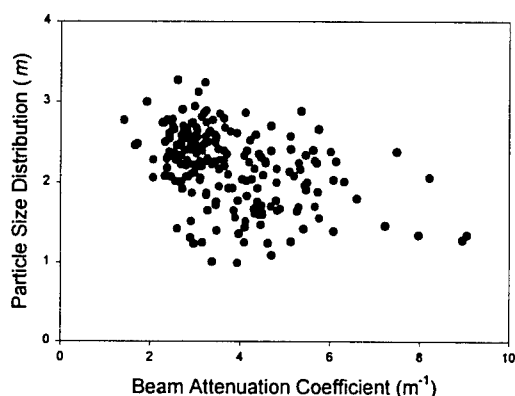

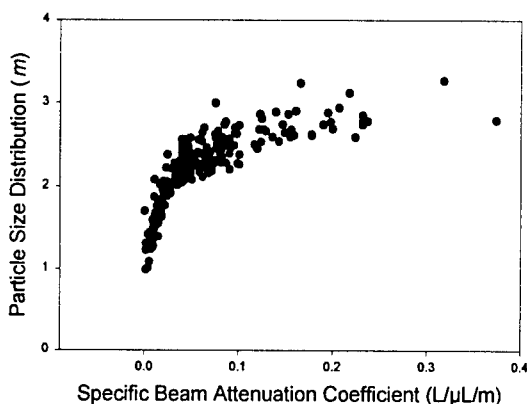Figure 19: PSD vs. *c* shows no delineation with respect to time, depth, or geography.

Figure 20: The PSD has a strong impact on *c**, thereby explaining the significant scatter found in Fig 18.

D. Scattering and Absorption

As the absorption due to biological particulates is primarily due to *chlorophyll a* *(chl a)*, the spectral absorption characteristics can be expected to be similar to the absorption of that pigment (Fig 21). While there is obviously deviation from this due to the presence of other biological pigments, the construct of the absorption spectrum due to biological particles in most natural waters remains structurally similar to the *chl a* spectrum (Fig 22). The absorption spectrum attributed to CDOM and detrital particles is similar in shape and simply an exponential decrease in absorption with wavelength (Fig 23). The absorption characteristics of *chl a*, CDOM, and detrital particles, all of which are intrinsically related to biological activity, are the dominate contributors to *in situ* absorption spectra. Therefore, biological particles dominate absorption variation.

The single-scattering albedo (*w*), is the ratio (*b/c*) of the scattering coefficient to the beam attenuation. As measured by Petzold (1972), a characteristic value of the single scattering albedo for the open ocean is 0.247, 0.551 for a coastal regime, while a turbid harbor (San Diego) has the highest value of 0.833 at 530nm. As measured by the AC-9 at 555nm, the average single-scattering albedo for this study was approximately 0.91. This extremely high value demonstrates both how scattering-dominated these waters are, and how optically different from those in past studies. The single-scattering albedo shows a slight trend in relation to total suspended volume (Fig 25), suggesting that absorption varies widely when the suspended load is lighter and is less significant at heavier loads. Additionally, the single-scattering albedo shows a dependence on the particle-size distribution. Absorption appears to contribute more to the beam attenuation
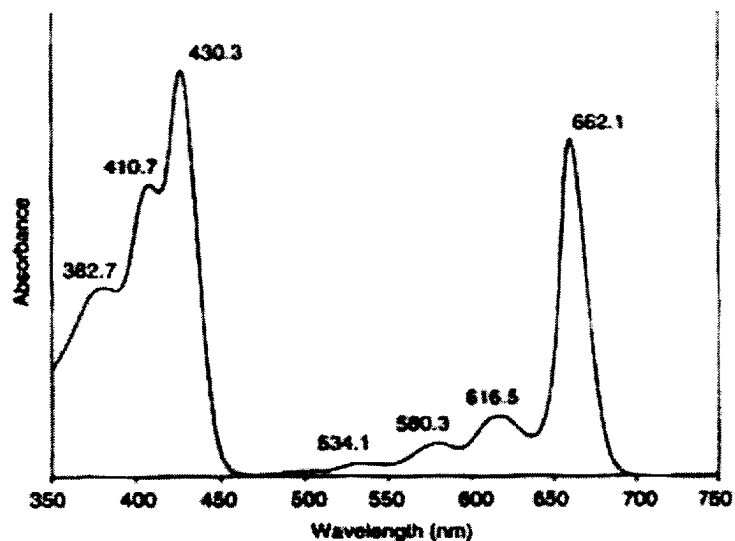
Figure 21: *Chlorophyll a* absorption as determined by High Pressure Liquid Chromatography. Notice the absorption peaks at 430nm and 662nm.
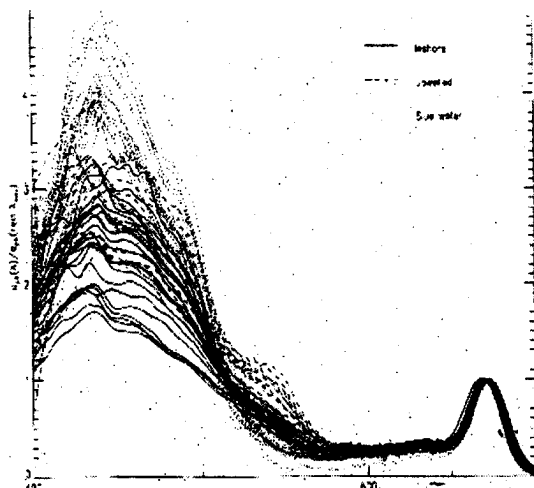

Figure 22: Particulate absorption curves for a variety of natural waters (normalized at 676nm). The major absorption peaks corresponding to *chlorophyll a* dominate the spectral shape.
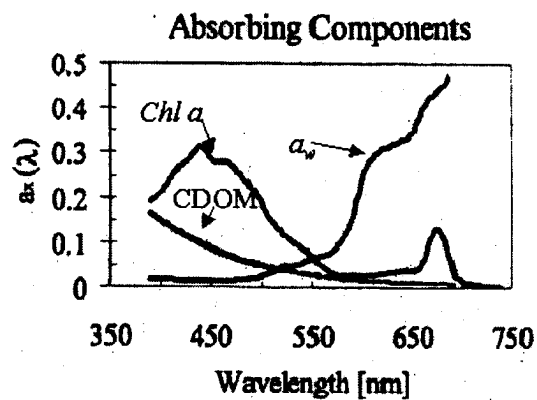

Figure 23: Typical absorption spectra for *chlorophyll a*, CDOM, and pure water.

in particle-size distributions that are skewed toward smaller particles (Fig 24). This relationship holds true for all wavelengths.

Aside from a particle-size distribution and total suspended volume dependence, the single-scattering albedo also demonstrates depth dependence. Looking at $w(676)$, the single scattering is clearly greater at depth than at the surface (Fig 26). This is true with the exception of 10 November and 1 October, when the dependence has broken down.
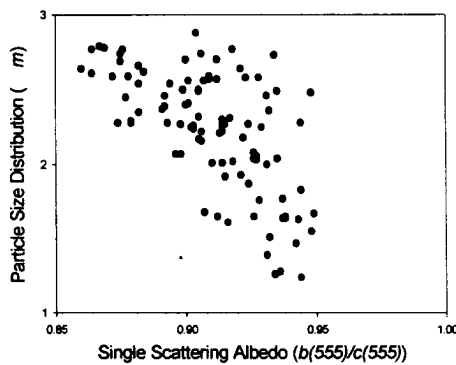

Figure 24: Single scattering albedo ($w(555)$) plotted against PSD shows a very general relationship between w and PSD.
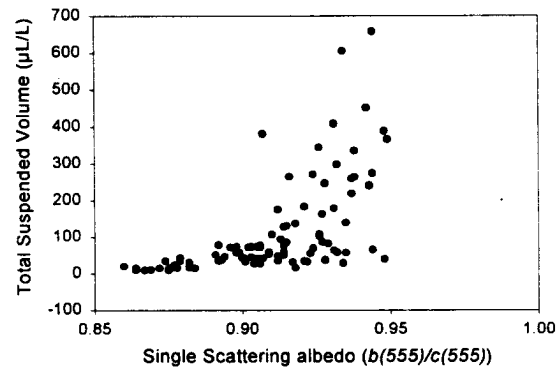

Figure 25: Single scattering albedo ($w(555)$) plotted against TSV shows a slight inverse relationship.

Comparing this with a time series of the scattering coefficient shows that the depth dependence is not a function of the change in the scattering coefficient (Fig 26). The absorption time series, however, shows a similar dependence with depth as the single scattering albedo at 676nm (Fig 26). Since 676nm is near an absorption peak of *chl a*, it is likely this decrease in the absorption coefficient and increase in the single-scattering albedo with depth is a result of a decreasing concentration of biologics with depth. The depth dependence of absorption at 676nm also breaks down slightly on 10 November and
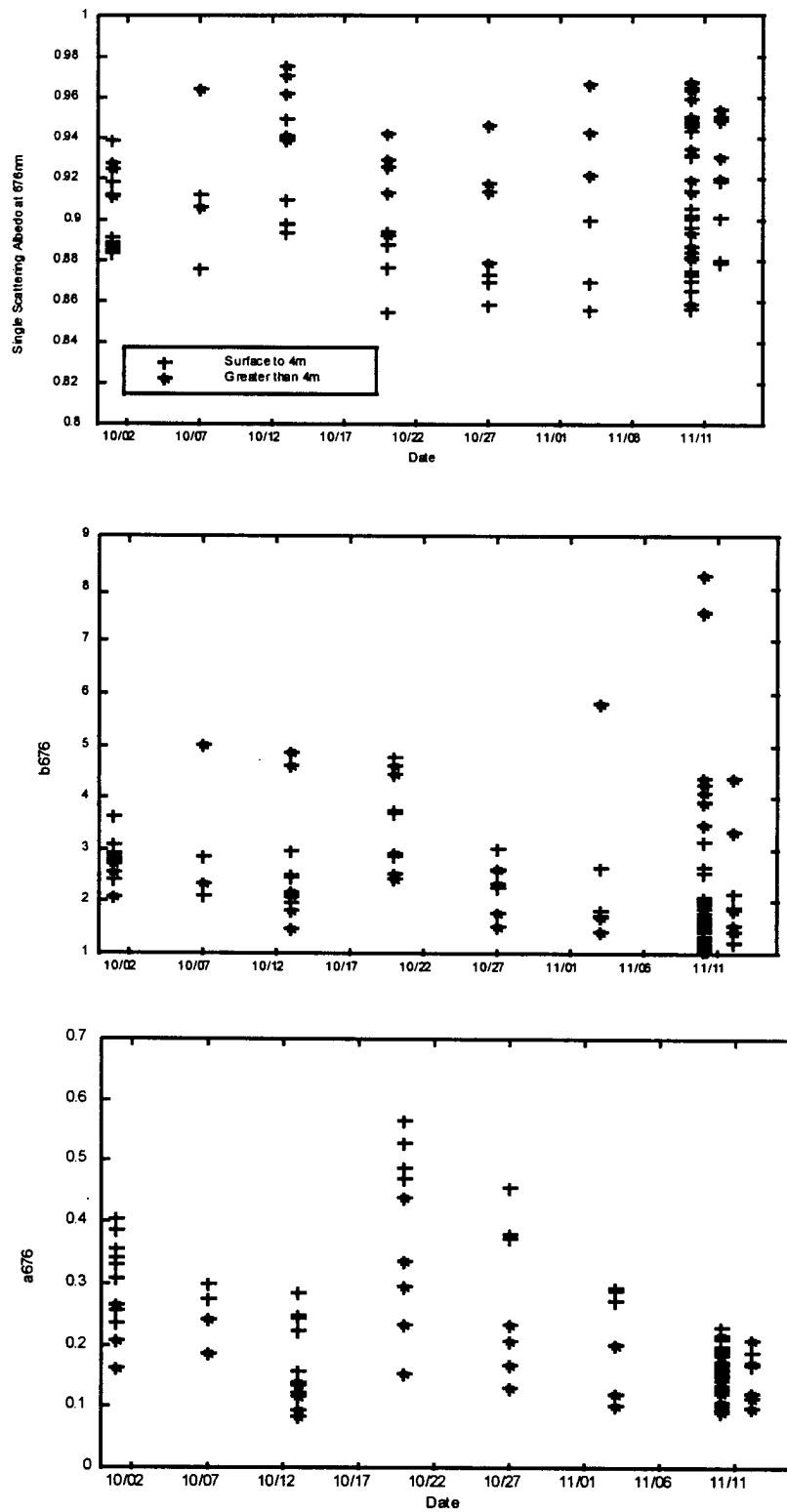
Figure 26: Single scattering albedo, scattering, and absorption at 676nm separated by depth.
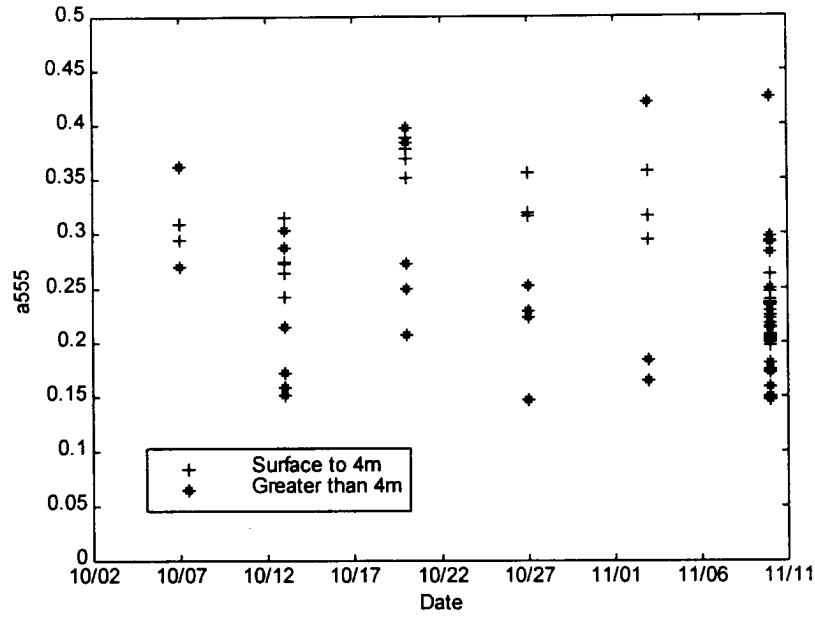
Figure 27: Absorption at 555nm in time shows no appreciable depth distinction.
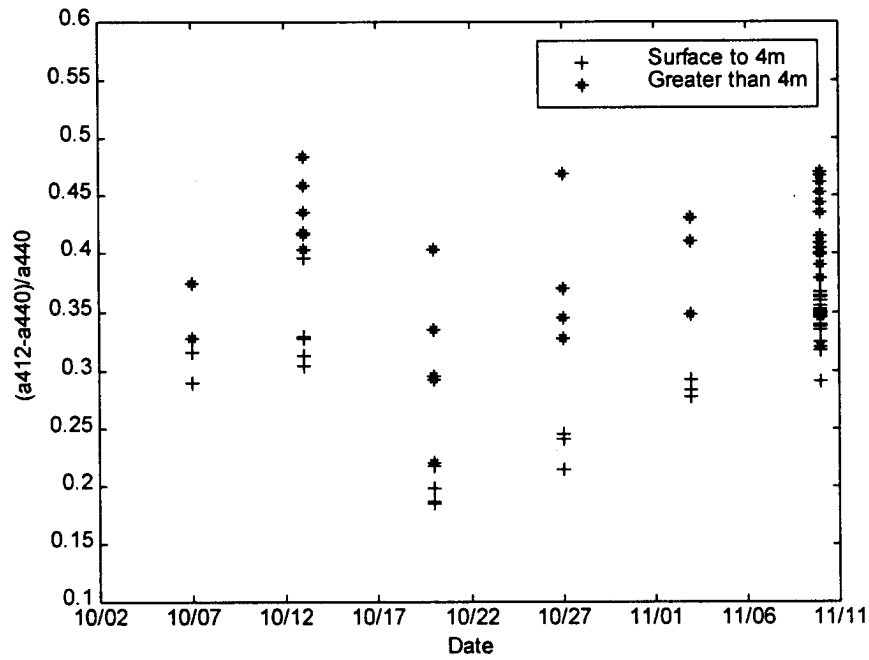

Figure 28: The percent difference between *a412* and *a440*, which is proportional to the combined effects of CDOM and detrital absorption, shows clear distinction with depth.

1 October, explaining the breakdown in the scattering-albedo depth dependence on that

depth. Additionally, the dependence breaks down if the wavelength is changed to

555nm, where chlorophyll does not absorb as strongly (Fig 27). However, the depth

dependence is also deteriorated at 412nm for all time. As chlorophyll is expected to

absorb strongly at 412nm, this suggests that detrital or CDOM variation is influencing the

dependence of absorption on depth. In the east-west direction, $w(676)$ suggests that

absorption plays a more significant role at the lateral boundaries of the Bay (Fig 29).
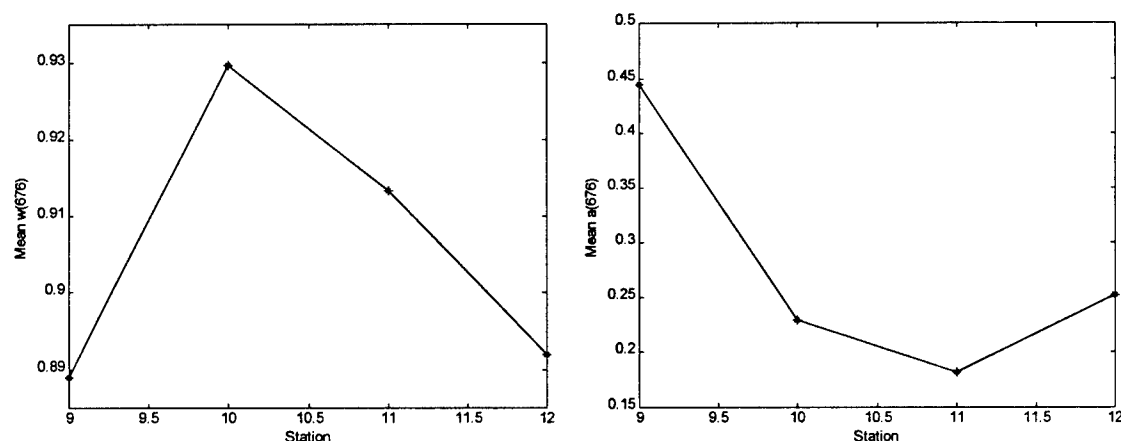
Figure 29: The west to east variation in the single scattering albedo and absorption at 676nm.

Absorption variation at that wavelength confirms that chlorophyll is more prevalent at the

boundaries (Fig 29).

For the wavelengths used in this study, CDOM and detrital absorption will be

strongest in the 412nm waveband. Chlorophyll or biologic absorption, however, will be

strongest at 440nm. The difference between the absorption at these two wavebands

normalized to the 440 band can be used as a proxy for the concentration of CDOM or

detrital material with:

$$a_{CDOM} \propto \frac{a(412) - a(440)}{a(440)}.$$ (13)

This proxy shows a clear dependence upon depth (Fig 28). As depth increases, the absorption at 412nm increases over the absorption at 440nm. This suggests either increasing CDOM or detrital concentrations with depth.

The scattering coefficient shows a strong dependence upon the total suspended volume. The beam attenuation data also correlate well with the total suspended volume for 7-20 October. For the same time span, the scattering coefficient shows a high correlation coefficient ($r^2 \approx 0.72$) and a slope of 71 $\mu L/L/m^{-1}$ (Fig 30). The slope of 71 $\mu L/L/m^{-1}$ compares well with the beam attenuation slope of 87 $\mu L/L/m^{-1}$. The absorption coefficient shows no correlation for this period ($r^2 < 0.1$). The next particulate
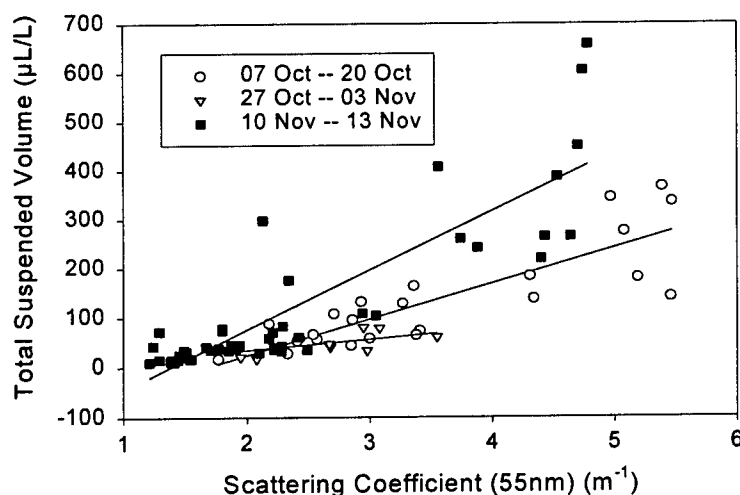
Figure 30: Relationship between the scattering coefficient and TSV showing clear changes in the relationship and increased correlation.

regime continues until 3 November and does not show a strong correlation between TSV and b. The low slope of 22 μL/L/m^{-1} is comparable to the beam attenuation correlation; however the r^2 is only 0.42. Beginning with 10 November, however, the correlation increases dramatically to 0.76 and the slope of 130 μL/L/m^{-1} is understandably very close to the beam attenuation slope of 127 μL/L/m^{-1}. The absorption coefficient showed no correlation in any of the regimes.

E. Scales of Variability

The index of refraction of the suspended particulates, particularly the specific scattering coefficient, has been shown to covary with stratification and destratification. The distribution of particle concentration, however, may vary on much shorter time scales due to tidal and other advective processes and cause significant variation in the optical properties. The degree of this variation has important implications on the feasibility of utilizing optical remote sensing systems.

Considering the semi-diurnal tidal variation in the Chesapeake, variability in the optics over the span of several hours may be attributed to changes in the vertical current structure. On 1 October, two casts at station 11 separated by about three hours show only minor variation in the density profile (Fig 31a). The variation in beam attenuation coefficient, however, is quite pronounced (Fig 31b). ADCP data taken at previous station 11 casts indicate the presence of a current jet at 10 to 15 meters of depth at varying tidal stages. The clear water intrusion centered at 11 meters on the afternoon cast is likely attributable to the presence of that jet. A sharp turbidity maximum occurs immediately beneath the clear water intrusion. Over the course of three hours, significant vertical structure develops in the beam attenuation coefficient. At any depth the beam attenuation coefficient may change by as much as 0.5 m^{-1}.

Over much shorter time scales, vertical oscillations such as internal waves in the water column may impose meaningful changes in the beam attenuation structure. Station 9 was sampled with a 20-minute spacing on 30 September. Changes in the density structure indicate about one meter of vertical movement of the bottom layer toward the surface (Fig 32a). The vertical change in the beam attenuation coefficient is quite

pronounced throughout the water column with as much as a meter rise in the turbidity minimum (Fig 32b). This vertical movement appears to compress the surface layer, thereby raising the value of the surface turbidity maximum and increasing the slope of decline of beam attenuation with depth until the turbidity minimum is reached. Conversely, raising the bottom layer lessened the slope of increase of beam attenuation toward the bottom turbidity maximum.
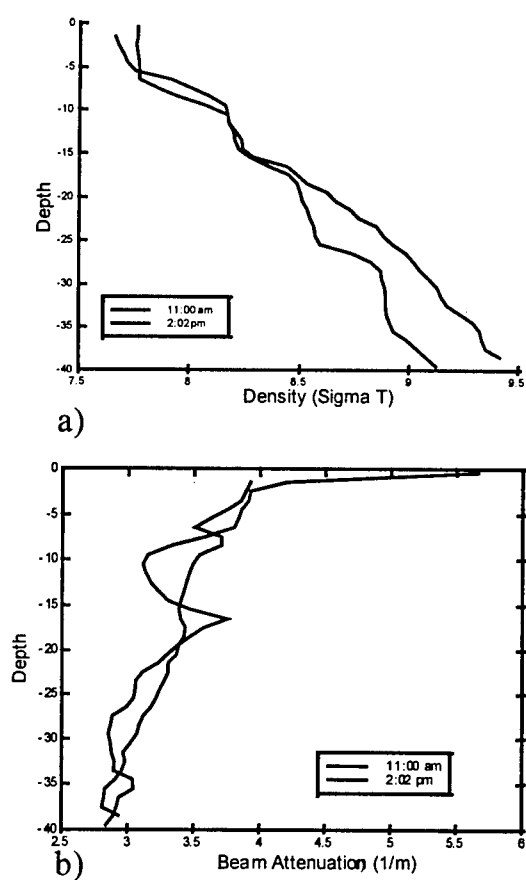
Figure 31: Changes in the structure of the a) density and b) beam attenuation profiles at station 11 over the course of three hours.

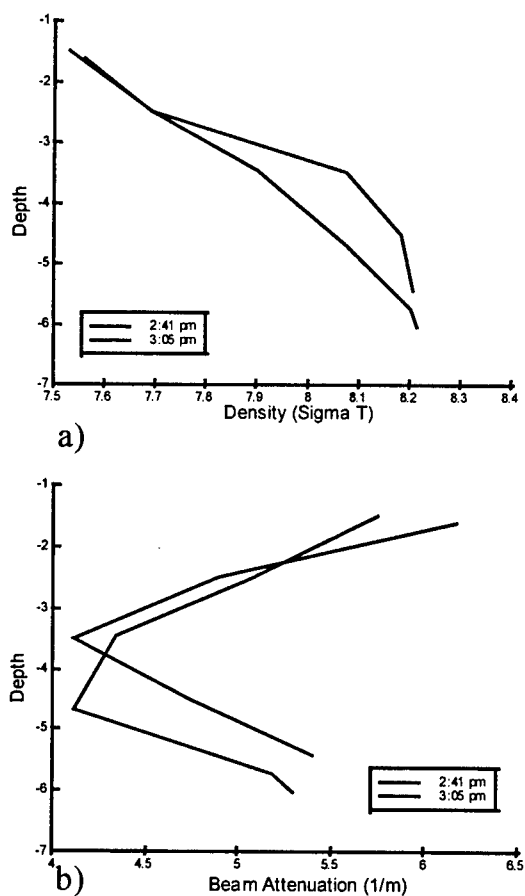Figure 32: Changes in the structure of the a) density and b) beam attenuation profiles at station 09 over a twenty-minute time-span.
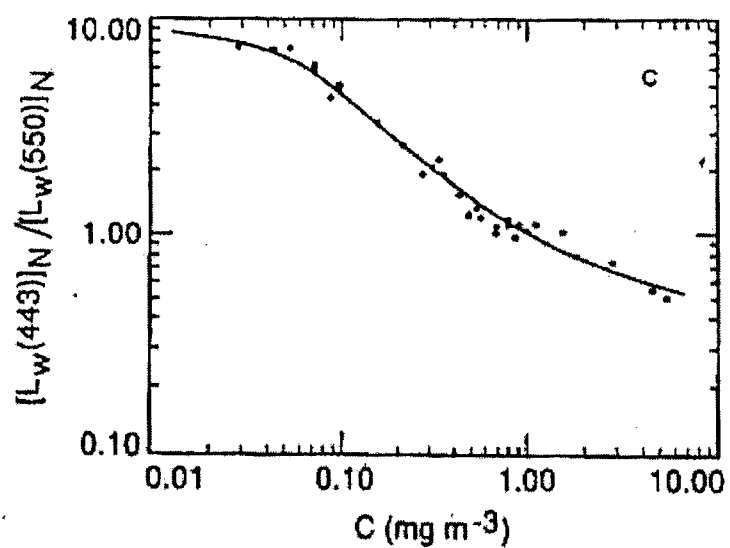
Figure 33: The relationship between the water-leaving radiance ratio at 443nm and 550nm and *chlorophyll.* (Gordon, 1983)
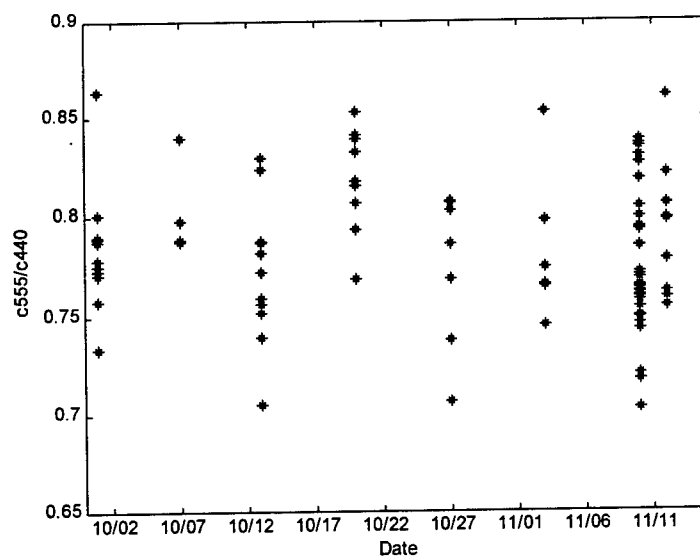

Figure 34: Test of the application of the 443/555 remote sensing inversion ratio by using *c555/c440*. No discernible relationship to hydrographic phases exists.

F. Remote Sensing

F. 1. Traditional Ratios

Optical remote sensing devices record the intensity of a particular waveband of light leaving the water at a particular angle, or the water leaving radiance (L_w). Algorithms are then used to invert these intensities into the inherent optical properties of the water column (i.e., c, a, and b), and then further to the properties of the suspended particulates (i.e. biomass and *Chl* concentrations). These algorithms often involve ratios of wavelengths. For example, the ratio of normalized water leaving radiance at 443nm and 555nm was used to invert Coastal Zone Color Scanner (CZCS) image data into chlorophyll concentrations (Fig 33) (Gordon and Morel, 1983). Furthermore, many inversion schemes are heavily dependent on absorption and backscattering, mostly in the ratio:

$$\frac{b_b}{a + b_b}. \tag{14}$$

The optical properties of the Chesapeake as outlined in this study suggest that these algorithms will be of little use in the Bay. The ratio of beam attenuation at 555nm to that at 443nm should be roughly inversely proportional to the 443nm to 555nm water leaving radiance ratio. Similarly, absorption at 676nm can be used as a proxy for chlorophyll concentration. Relating these quantities yields no relationship (Fig 34), suggesting that CZCS algorithm does not work in this environment. Furthermore, the magnitude of the absorption coefficient shows no appreciable variation with destratification/stratification. While there are changes in absorption which suggest that increases in chlorophyll concentration may be discernible, the small scale of variability

with regard to concentration and hence absorption magnitude suggests that interpreting absorption changes with remote sensing imagery may be difficult.

F. 2. Backscattering effects

Remote sensing imagery is also heavily dependent upon backscattering. The magnitude of backscattering, which is a difficult quantity to measure, is often taken as a specified form of the scattering coefficient when used in these models. The specific scattering coefficient showed considerable variation with destratification/ stratification. However, this distinction did not exist for the scattering coefficient due to variation in concentration. This suggests that neither the absorption nor the backscattering coefficient show variation across mixing events. Therefore, using these assumptions, the capabilities for remote-sensing imagery to delineate these events is suspect.

F. 2. a. Weighting function

Modeling using Mie theory, however, suggests that the assumption that backscattering can be computed as a fraction of the total scattering coefficient is most likely invalid in the Chesapeake Bay. The value of any integrated optical quantity (the backscattering coefficient, for example), is simply the sum of effects of each particle size:

$$b_b = \Sigma \left(N(\alpha) \cdot Q_{b_b}(\alpha, n) \cdot \pi \cdot \alpha^2 \right) \tag{15}$$

where $N(\alpha)$ is the number of particles in the size-bin centered on Mie size-parameter α, Q_{bb} is the backscattering efficiency, n the index of refraction (where the real component has a scattering effect and the imaginary component an absorption effect), and the

summation is performed over the entire size distribution. As $N(\alpha)$ can be represented by a Junge distribution, the contribution of any size range centered on α to the integrated quantity becomes strictly a function of the slope of the particle-size distribution and the index of refraction. Furthermore, changing the index of refraction, especially with regard to smaller particles, affects primarily the magnitude and the shape of the Q_{bb} curve (Fig 35). Therefore, a reliable weighting function describing the contribution of each particle-size bin to the integrated value can be generated for a given particle-size distribution.

The weighting function shows that particle-size ranges contributing to the integrated quantity vary considerably with the particle-size distribution. As particle-size distributions skew toward smaller particles (the slope becomes greater than two), the backscattering signal becomes almost entirely comprised of the effect of the smallest particles in the size distribution (Fig 36).
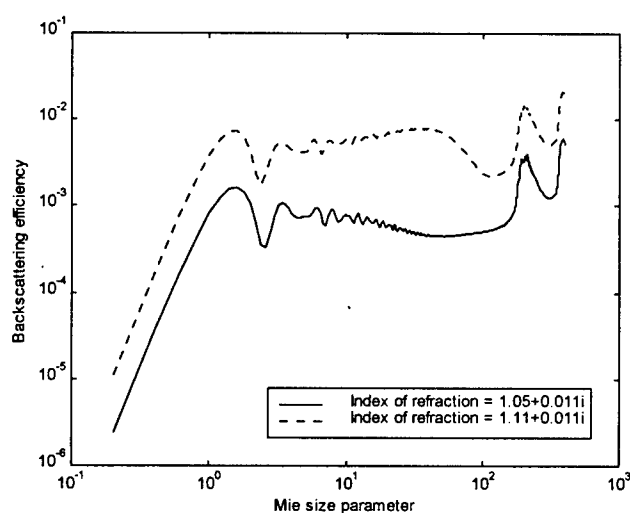
Figure 35: Variation in the backscattering efficiency due to changing indicies of refraction. There is very little variation in the shape of the function at small particle sizes
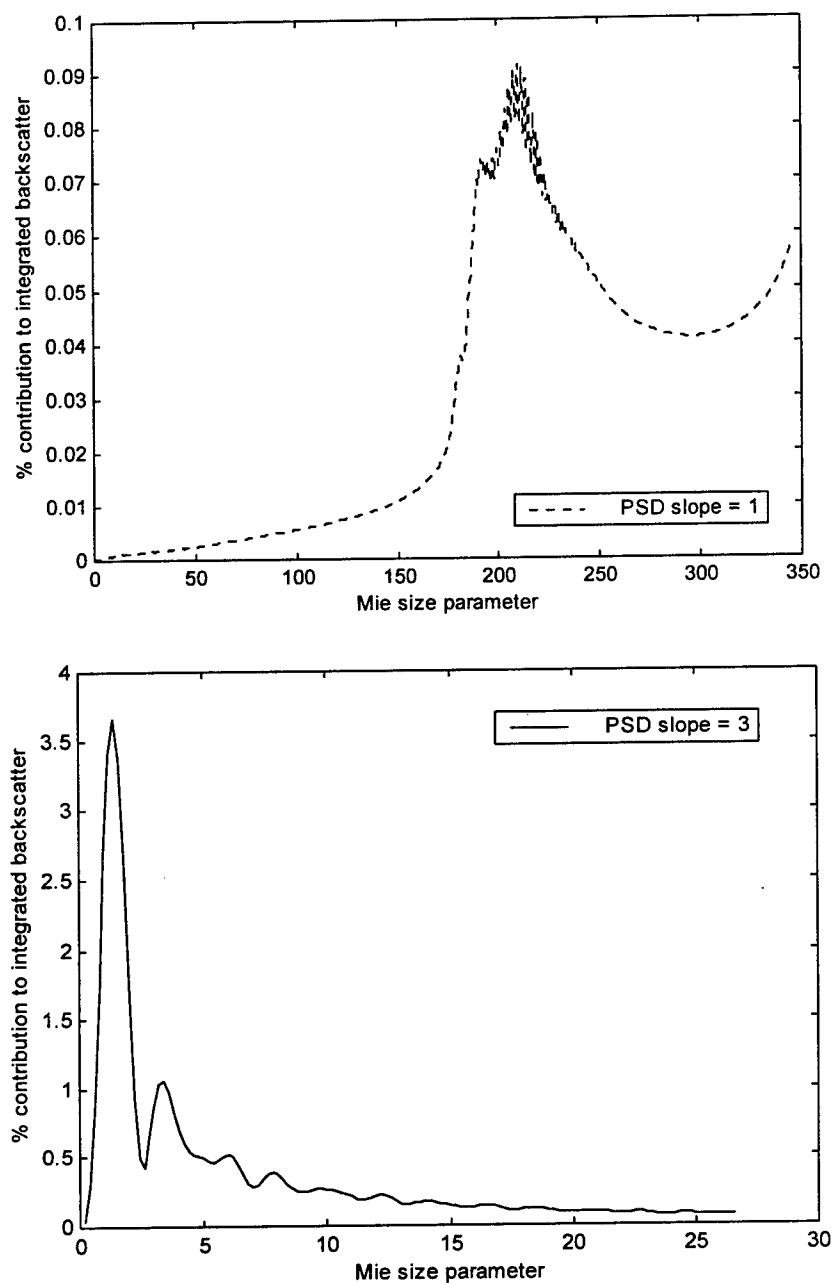
Figure 36: Weighting functions showing the particles that comprise 50% of the integrated signal and their relative weights. Particle sizes used in the creation of this weighting function range from 0.2-400 Mie size parameters. At top, for a PSD slope of one, 50% of the signal comes from the largest 300-400 Mie size parameter particles, while at bottom, for a PSD of 3, the majority of the signal comes from particles less that 27 in Mie size parameter.

F. 2. b. Impact on remote sensing

The relationship between the single-scattering albedo and the particle-size distribution indicates that absorption was more significant in distributions skewed toward smaller particles. As variation in the PSD has been shown to be due to addition/subtraction of large particles, it is probable that the smaller particles are of a different index of refraction than the larger, thereby explaining the variation in single scattering albedo. These particles may have significantly different backscattering properties than their larger counterparts that dominate the forward scattering. Therefore, backscattering does not necessarily covary with the scattering coefficient.

As a result of this ambiguity in the backscattering variation, a discernible remotely sensed signal may exist for destratification resulting from a change in backscattering properties independent of changes in the scattering coefficient. However, considering the degree of variation in the particle size distribution, which appears somewhat stochastic, it can be expected that the backscattering coefficient will not be able to delineate the stratification/destratification boundary. Therefore, utilizing current techniques and wavebands, it is highly unlikely that remote sensing imagery can be properly interpreted to invert water-leaving radiance into inherent optical properties.

VI. Discussion

The hydrographic and optical data indicate that the Bay is extremely dynamic during the fall season. Initial destratification occurred on 15-16 September. A temperature inversion was in place before destratification could occur. The more intense storm beginning on 7 September did not induce destratification. This is most likely due to the southerly (up the Bay) direction of the winds enhancing gravitational circulation and thereby strengthening the halocline.

The mixing event is accompanied by a considerable increase in the specific beam attenuation coefficient (the beam attenuation coefficient per unit total suspended volume, c^*). The hydrography of the water column remained destratified through 1 October. Similarly, the specific beam attenuation coefficient maintained a high value throughout that period. Beginning on 7 October and lasting through 20 October, the hydrographic data indicate restratification. The specific beam attenuation coefficient correspondingly decreased for that period. As mixing occurred again on 27 October, the c^* reached its highest value. Following the onset of stratified conditions on 10 November the specific beam attenuation lowered again.

The linear relationship between beam attenuation and total suspended volume, without a corresponding distinction in the beam attenuation and particle-size distribution relation, suggests that the composition of the suspended load does not appreciably vary with depth or geographic distribution. However, absorption data indicates a decreasing contribution to the optical signal by phytoplankton with depth. Similarly, absorption information indicates a relative increase in detrital particles or

CDOM with depth. Both of these events impose a change on the composition of the particulate load.

The high value of the single-scattering albedo and the high correlation of the scattering coefficient to the total suspended volume indicate that optical variation is dominated by changes in the scattering properties of the suspended load. Specifically, destratification results in a significant increase in the real index of refraction of the suspended load. This increases the specific scattering coefficient of the suspended load, which dominates variation of the specific beam attenuation coefficient. Furthermore, the index of refraction of optically significant scatters does not vary appreciably with depth or geographic distribution. Therefore, the major cause of variation in the beam attenuation coefficient is changes in the concentration of these scatterers within the water column.

While scattering is the major optical variable, absorption has demonstrable effects upon the specific beam attenuation coefficient. The time series of $a(676)$ (Fig 26) shows a considerable increase in absorption on 20 October. As the scattering coefficient shows little to no variation, the absorption increase is most likely attributable to a bloom in phytoplankton concentrations between 13 and 20 October. Separating this date from the other stratified points shows clear distinction and increase in the specific beam attenuation coefficient.

VII. Conclusions

The physical dynamics of the Chesapeake Bay during the fall are heavily dependent upon the prevailing meteorology. Decreasing atmospheric temperatures create a pynocline weakening temperature inversion. Once the temperature inversion is in place, the vertical structure of the Bay is heavily dependent upon the winds associated with storm systems. The magnitude and direction of these winds affect the stratification conditions, with strong southerly winds promoting mixing and strong northerly winds advancing gravitational circulation and promoting stratification.

The concentration and particle-size distribution of suspended particulates vary extensively with depth and geography in the Bay, with larger particles comprising the majority of the variation. Particle concentrations generally decrease and size distributions skew toward smaller particles moving west to east across the Bay.

The Chesapeake during the autumn is optically scattering dominated with single-scattering albedos ranging from 0.85 to 0.95. The specific scattering properties of the water column do not vary geographically or with depth. The scattering properties of the suspended particulates show distinct shifts in time, which appear to be correlated to mixing/stratification processes. The scattering dominates the beam attenuation, which therefore shows a similar shift.

The absorption properties of the water column clearly show both depth and geographic variation, suggesting a strong dependence upon biological activity. Spectral absorption information appears to be capable of distinguishing chlorophyll containing particulates from detrital material and CDOM, despite the high single-scattering albedo.

The significant variation in the concentration and particle-size distribution of the suspended load over small time scales suggests that traditional inversion methods for remotely sensed radiances can not be applied in the Chesapeake. While it is probable that the backscattering coefficient will vary independent of changes in the specific scattering, this will likely not improve the ability to develop an algorithm for the inversion remote sensing imagery.

VIII. Future Study

Further study demands a detailed analysis of the particulates comprising the suspended load. In particular, the change in character of larger particles across the destratification event needs to be studied on the individual particle level. Additionally, in order fully utilize absorption spectrum, a detailed study utilizing High Pressure Liquid Chromatography (HPLC) needs to be performed, as it is likely that the pigments contributing to the absorption spectrum are considerably different from those in open ocean and coastal waters. In general, more temporally dense absorption and scattering measurements are required.

IX. Naval Applications

The Navy has a considerable interest in this type of research. The processes covered in detail in this study may form the foundation of any predictive model for water clarity.

The ability to accurate predict water clarity is important for both the special warfare and mine warfare. For special warfare, water clarity is critical to detection ranges and with regards to diver navigational ability. These requirements are important to the point that the special warfare community listed optical oceanography as a requested area of research in the National Research Council symposium on Oceanography and Naval Special Warfare (1997). Additionally, a large portion of mine warfare is conducted through visual means.

Beyond strictly water clarity models, a predictive capability for inherent optical property variation is also of interest to the US Navy. Laser bathymetric and anti-submarine warfare (ASW) systems, which are increasing in number and application, require this information in order to predict detection depths and signal-to-noise ratios.

As the mission of the Navy has brought it into the littoral regime, it is likely that a requirement for laser dependent mine detection or water clarity prediction for special forces insertion will develop in an optical regime dominated by scattering and similar to the Chesapeake. This research represents a fundamental early step toward these capabilities.

X. Bibliography

AC-9 Protocol. 1998. WETLabs Inc. Philomath, Oregon.

Bader, H. 1970. The hyperbolic distribution of particle sizes. *Journal of Geophysical Research*, 75(15), 2822.

Bohren, C.F, and D.R. Huffman. 1983. *Absorption and Scattering of Light by Small Particles*. Canada: John Wiley and Sons.

Chandrasekhar, S. 1960. *Radiative Transfer*. New York: Dover Publications.

Coleman, J.E. and R. W. Spinrad. 1998. "Optical variability in the northern Chesapeake Bay", *Proceedings of the Ocean Community Conference '98 (CD-ROM)*. Marine Technology Society, Washington, DC, 5pp.

Goodrich, D.M., W.C. Boicourt, P. Hamilton, and D.W. Pritchard. 1987. Wind-induced destratification in the Chesapeake Bay. *Journal of Physical Oceanography*. 17.

Gordon, H.R., and A.Y. Morel. 1983. *Remote assessment of ocean color for interpretation of satellite visible imagery, A review*. New York: Springer.

Gordon, H.R., D.K. Clark, J.W. Brown, O.B. Evans, R.H. Evans, and W.W. Broenkow. 1983. Phytoplankton pigment concentrations in the Middle Atlantic Bight: A comparison of ship determinations and CZCS estimates. *Applied Optics.*, 22.

Hamilton, M., T.C. Granata, T.D. Dickey, J..D. Wiggert, D.A. Siegel, J. Marra, and C. Langdon. 1990. Diel variations of bio-optical properties in the Sargasso Sea. *SPIE Ocean Optics X* 1302: 214-224.

Holm-Hansen, O., C.J. Lorenzen, R.W. Holmes, and J.D.H. Strickland. 1965. Fluorometric determination of chlorophyll. *J. Cons. Perm. Int. Explor. Mer.* 30.

Irwin, C.S., M.E.C. Vieira, and R. Malek-Madani. 1997. *Dynamics of destratification in the Severn River estuary: U.S.N.A. Trident Scholar project report*, 248.

Jerlov, N.G., 1976. *Marine Optics*. Elsevier Scientific Publishing Company

Kirk, J. T.O. 1994. *Light and Photosynthesis in Aquatic Ecosystems*, Cambridge University Press.

Mie, G. 1908. Beitrage zur Optik truber Medien speziell kolloidaler Metallosungen, *Annulls Physik* 22:351-362.

Mitchell, B.G. 1990. Algorithms for determining the absorption coefficients of aquatic particles using the quantitative filter technique (QFT). *SPIE Ocean Optics X* 1302: 137-148.

Ocean Studies Board, National Research Council. 1997. *Oceanography and Naval Special Warfare: Opportunities and Challenges*. National Academy Press.

Pegau, W.S., J. Cleveland, D. Kennedy, J.L. Mueller, R.A. Maffione, C. Trees, K.J. Voss, A. Weidemann, W. Wells, and J.R.V. Zaneveld. 1995. "A comparison of methods for the measurement of the absorption coefficient in natural waters." *Journal of Geophysical Research* 100:13,163-13,178

Petzold, T.J. 1972. Volume scattering functions for selected ocean waters, SIO Ref. 72-78, Scripps Inst. Oceanogr., La Jolla, 79 pp. Condensed as Chapter 12 in *Light in the Sea*, Ed J.E. Tyler, Dowden, Hutchinson, Ross, Stroudsberg, 1977.

Pritchard, D. W. 1989. Estuarine classification -- a help or a hinderance. *Estuarine Circulation*, Neilson, B.J. et al. Ed. Humana Press.

Roesler, C. S. Theoretical and experimental approaches to improve the accuracy of particulate absorption coefficients derived from the quantitative filter technique. *Limnology and Oceanography*, preprint, 1998.

Seabird CTD Protocol, Seabird Electronics. Bellevue, Washington.

Smith, D.E, Leffler, M., and Mackiernan, G. 1992. *Oxygen Dynamics in the Chesapeake Bay*. Maryland Sea Grant College.

Spinrad, R. W. 1986. Use of the specific beam attenuation coefficient for identification of suspended particulate material. *SPIE Ocean Optics VIII* 637.

Tyler, M. A. and H.H. Seliger. 1989. Time scale variations of estuarine stratification parameters and impact on the food chains of the Chesapeake Bay. *Estuarine Circulation*, Neilson, B.J. et al. Ed. Humana Press.

van de Hulst, H.C., 1957. *Light Scattering by Small Particles*. John Wiley & Sons.

Vieira, M.E.C., 1986. The meteorologically driven circulation in mid-Chesapeake Bay. *Journal of Marine Research*, 44. 473-493.

Zaneveld, J.R.V., J.C. Kitchen, A. Bricaud, and C.C. Moore. 1992. Analysis of in-situ spectral absorption meter data. *SPIE Ocean Optics XI* 1750: 330-337.